Computer Physics Communications 184 (2013) 2571–2587

Contents lists available at ScienceDirect

Computer Physics Communications

journal homepage: www.elsevier.com/locate/cpc

GTROTA: A code for the solution of the coupled nonlinear extended neoclassical rotation equations in tokamak plasmas using successive over-relaxation and simulated annealing☆

C. Bae [a,c,*], W.M. Stacey [a], T.D. Morley [b]

[a] Fusion Research Center, Nuclear and Radiological Engineering, Georgia Institute of Technology, Atlanta, GA 30332-0740, USA
[b] School of Mathematics, Georgia Institute of Technology, Atlanta, GA 30332-0160, USA
[c] National Fusion Research Institute, Daejeon 305-333, South Korea

ARTICLE INFO

Article history:
Received 16 October 2012
Received in revised form
19 March 2013
Accepted 10 June 2013
Available online 20 June 2013

Keywords:
Nonlinear
Tokamak
Plasma
GTROTA

ABSTRACT

GTROTA (Georgia Tech ROTAtion) is a code that solves the extended neoclassical rotation equations for tokamak plasmas, derived from the multifluid moment equations (including electromagnetic effects) in generalized toroidal magnetic flux surface geometry. It computes the toroidal and poloidal fluid rotation velocities and the in–out and up–down density asymmetries at each radial location. The solution of these equations is accomplished iteratively, using a physically motivated decomposition, successive over-relaxation and the concept of simulated annealing.

Program summary

Program title: GTROTAv1
Catalogue identifier: AEPT_v1_0
Program summary URL: http://cpc.cs.qub.ac.uk/summaries/AEPT_v1_0.html
Program obtainable from: CPC Program Library, Queen's University, Belfast, N. Ireland
Licensing provisions: Standard CPC licence, http://cpc.cs.qub.ac.uk/licence/licence.html
No. of lines in distributed program, including test data, etc.: 12 890
No. of bytes in distributed program, including test data, etc.: 1 099 937
Distribution format: tar.gz
Programming language: Matlab.
Computer: Any workstation or PC where Matlab can be run.
Operating system: Any with Matlab available. Tested on Windows 7.
RAM: 1024 MB to run Matlab
Classification: 19.11.

Nature of problem:
Tokamak plasma rotation velocities and the poloidal in–out and up–down asymmetries of plasma densities are calculated from the coupled set of nonlinear equations, which show a very instable iterative dynamics. To solve for the true solution for this nonlinearly coupled system that does not converge to a single solution, physics-based determination of the true solution becomes necessary and GTROTA provides the algorithm for users to find the true solution from the nonlinear topological maps.

Solution method:
The code decomposes the given system into three subsystems to stabilize the iterative dynamics and uses Successive Over-Relaxation and the concept of Simulated Annealing to determine the true solution.

Restrictions:
The code is designed for strong rotation analysis. An updated code for slow rotation and plasma edge analysis is to be developed in the future.

☆ This paper and its associated computer program are available via the Computer Physics Communication homepage on ScienceDirect (http://www.sciencedirect.com/science/journal/00104655).

* Correspondence to: 113 Gwahak-ro, Yuseong-gu, Daejeon, 305-333, South Korea. Tel.: +82 10 2168 0825.
E-mail addresses: cbae@nfri.re.kr (C. Bae), weston.stacey@nre.gatech.edu (W.M. Stacey), morley@math.gatech.edu (T.D. Morley).

0010-4655/$ – see front matter
http://dx.doi.org/10.1016/j.cpc.2013.06.006

Unusual features:
For a new rotation calculation, the code requires several test runs to determine the iterations step for the true solution.

Additional comments:
Due to the extreme nonlinearity of the extended rotation calculation model, the signs of the inputs must be adjusted correctly to yield correct solutions. Refer to the User's Manual for this discussion.

Running time:
8 s (except test runs that depend on the complexity of the nonlinear dynamics).

1. Introduction

The extended neoclassical rotation equations for tokamak plasmas are derived from the first two multifluid moments equations (continuity and momentum balance) by using the Braginskii decomposition of the magnetohydrodynamic viscosity tensor, a kinetic theory calculation of the viscosity coefficient, an analytical representation of the poloidal asymmetry of the toroidal magnetic flux surfaces, and a low order Fourier expansion of densities, flow velocities and electrostatic potential [1,2]. The resulting set of four equations per ion species, at each radial location, for the poloidal and toroidal fluid rotation velocities and the up–down and in–out asymmetries in ion density are coupled and nonlinear. While the basic equations are similar to the familiar fluid equations, they also include additional electromagnetic forces and a gyroviscosity term which are not present in the conventional fluid theory, and the generalized toroidal geometry of tokamak magnetic flux surfaces [3] introduces further interesting features.

The numerical solution of the resulting set of nonlinear equations confronts two challenges. One is the high vulnerability of the iteration algorithm to unstable iteration dynamics and the other is the identification of the true solution from the nonlinear topological maps generated by successive iterations. The former challenge was successfully controlled by decomposition on physical grounds of the set of coupled equations and the use of the Successive Over-Relaxation (SOR) method [4–6], while the latter challenge was successfully met by using the global minimization concept known as Simulated Annealing (SA) [7,8].

We note that an earlier version [9] of extended neoclassic rotation equations also took into account poloidal asymmetries, but used a simple "circular" toroidal magnetic flux surface geometry representation, whereas the equations solved in this paper are based on a more realistic representation of the non-circular magnetic flux surface geometry [3] and include an additional nonlinear term in the inertial term that was neglected in the previous extended neoclassical rotation equations [9]. Earlier neoclassical rotation theories [10–12] did not take into account the effect of poloidal asymmetries and the resulting nonlinearities, and while these lead to a simpler linear system of equations, these equations were not so successful in predicting the experimental rotation velocities as the extended neoclassical rotation equations [1].

The equations in this paper have been extended beyond the Hirshman–Sigmar [11]/NCLASS [10] equations (1) to solve the poloidal momentum balance equations not only for the poloidal velocity but also for the poloidal asymmetries in flow and density which allow the evaluation of the neoclassical gyroviscosity, and (2) to represent the poloidal asymmetry in the flux surface geometry using the Miller equilibrium model [3]. Orderings during the development are performed rather differently from the traditional method because the flux surface averages in general Miller geometry do not reduce to simple analytic forms and must be evaluated numerically. After getting the leading order expressions for each term in the momentum balance equation, all terms were combined and compared both analytically and numerically against each other and terms with smaller by at least two orders of magnitude from the leading terms are dropped to ensure accuracy in the calculation model. The development of the extended rotation formalism is discussed in detail with the comparison of the predictions of the code against experiment in Ref. [1].

2. Extended neoclassical rotation equations and the calculation model

2.1. Extended neoclassical rotation equations

The extended neoclassical rotation equations and its calculation model [1] is derived from the continuity,

$$\frac{\partial n_j}{\partial t} + \nabla \cdot (n_j \overrightarrow{V}_j) = S_j^o \tag{1}$$

and the momentum balance

$$m_j \frac{\partial}{\partial t}(n_j \overrightarrow{V}_j) + n_j m_j \nabla \cdot \left(\overrightarrow{V}_j \overrightarrow{V}_j\right) + \nabla P_j + \nabla \cdot \overleftrightarrow{\mathbf{\Pi}}_j = n_j e_j (\overrightarrow{E} + \overrightarrow{V}_j \times \overrightarrow{B}) + \overrightarrow{F}_j^{\,1} + \overrightarrow{S}_j^{\,1} \tag{2}$$

equations, where S is the source, P is the pressure, $\overleftrightarrow{\mathbf{\Pi}}$ is the viscosity tensor, and F is the collisional friction. The primary goal of the tokamak plasma rotation theory is to predict the toroidal and poloidal velocities of the main ion (deuterium), whose measurement is generally not available, and of the impurity ion (usually carbon), whose velocity is measured. The non-negligible poloidal and toroidal components of the inertial term in Eq. (2) are

$$\left[\left(\overrightarrow{V} \bullet \nabla\right)\overrightarrow{V}\right]_\theta = \frac{V_{\theta j}}{h_\theta}\frac{\partial V_{\theta j}}{\partial \theta} - \frac{V_{\theta j} V_{\phi j}}{h_\theta h_\phi}\frac{\partial h_\phi}{\partial \theta}, \tag{3}$$

$$\left[\left(\overrightarrow{V} \bullet \nabla\right)\overrightarrow{V}\right]_\phi = \left(\frac{V_{rj}}{h_r}\frac{\partial V_{\phi j}}{\partial r} + \frac{V_{\phi j} V_{rj}}{h_\phi h_r}\frac{\partial h_\phi}{\partial r}\right) + \left(\frac{V_{\theta j}}{h_\theta}\frac{\partial V_{\phi j}}{\partial \theta} + \frac{V_{\phi j} V_{\theta j}}{h_\phi h_\theta}\frac{\partial h_\phi}{\partial \theta}\right), \tag{4}$$

and of the viscosity terms with respect to Braginskii's viscosity representations [2,13–15] are

$$(\nabla \bullet \Pi)_\theta = \frac{1}{H}\frac{\partial}{\partial r}\left(Rh_\theta \Pi_{r\theta}\right) + \frac{1}{H}\frac{\partial}{\partial \theta}\left(h_r h_\phi \Pi_{\theta\theta}\right) - \frac{1}{h_\theta h_r}\frac{\partial h_r}{\partial \theta}\Pi_{rr} + \frac{1}{h_\theta h_r}\frac{\partial h_\theta}{\partial r}\Pi_{\theta r} - \frac{1}{Rh_\theta}\frac{\partial R}{\partial \theta}\Pi_{\phi\phi}, \tag{5}$$

$$(\nabla \bullet \Pi)_\phi = \left[\frac{1}{Rh_\theta h_r}\frac{\partial}{\partial r}\left(Rh_\theta \Pi_{r\phi}\right) + \frac{1}{Rh_r}\frac{\partial R}{\partial r}\Pi_{r\phi}\right] + \left[\frac{B_\theta}{h_\theta}\frac{\partial}{\partial \theta}\left(\frac{\Pi_{\theta\phi}}{B_\theta}\right) + \frac{1}{Rh_\theta}\frac{\partial R}{\partial \theta}\Pi_{\theta\phi}\right] \tag{6}$$

where $H = h_r h_\theta h_\phi$ with h_r, h_θ, and h_ϕ being the respective metric coefficients in (r, θ, ϕ) coordinate system. Braginskii decomposed the viscosity [15] into the parallel (η_{0j}), perpendicular (η_{1j}, η_{2j}), and gyroviscous (η_{3j}, η_{4j}) contributions, with viscosity coefficients

$$\eta_{0j} = \frac{n_j m_j V_{thj} q R_0 \varepsilon^{-3/2} \nu_{jj}^*}{\left(1+\varepsilon^{-3/2}\nu_{jj}^*\right)\left(1+\nu_{jj}^*\right)} \equiv n_j m_j V_{thj} q R f_j, \qquad \eta_{1j} = \frac{3}{10}\frac{n_j T_j}{\Omega^2 \tau}, \qquad \eta_{2j} = 4\eta_{1j}, \qquad \eta_{3j} = \frac{1}{2}\frac{n_j T_j}{\Omega}, \qquad \eta_{4j} = 2\eta_{3j} \tag{7}$$

where the collisional value of η_{0j} has been extended to include the banana–plateau region by using Shaing's result [2], and where V_{thj} is the thermal velocity of species j, q is the safety factor, $\nu = 1/\tau$ is the collision frequency with its normalized term $\nu^* \equiv \nu q R_0 / V_{th}$, and Ω is the gyrofrequency. The original Braginskii parallel viscosity coefficient (derived for a collisional plasma) has been extended to the above form for η_{0j} which takes into account the neoclassical trapped particle effects at small collisionalities and recovers the collisional result at large collisionalities. Since gyroviscosity arises from gyromotion, not collisions, the $\eta_{3,4}$ gyroviscosity coefficients are independent of collisionality".

Unlike earlier theories [10–12], in this extended neoclassical rotation model [1,9] the poloidal dependence is expanded for density and velocity in the lowest order Fourier series,

$$n_j(r,\theta) \approx \overline{n}_j(r)\left[1 + n_j^c \cos\theta + n_j^s \sin\theta\right], \tag{8}$$

$$V_j(r,\theta) \approx \overline{V}_j(r)\left[1 + V_j^c \cos\theta + V_j^s \sin\theta\right], \tag{9}$$

with the overbars indicating the values along the radial coordinate, thus introducing poloidal asymmetries ($n_j^{c,s}$ and $V_j^{c,s}$) in the formalism. Earlier models [10–12] did not include poloidal asymmetries in their formalism, and the experimental evidence is that these are not large; however we find [1] that inclusion of these poloidal asymmetries is important. Use of the Miller equilibrium geometry in the extended rotation theory [1] already includes poloidal asymmetries and the expansions in Eqs. (8) and (9) represent any further in–out and up–down asymmetries. The calculated results in Ref. [1] show that these further asymmetries are generally less than 10%, confirming validity of the model. Inclusion of further higher order poloidal asymmetries beyond Eqs. (8) and (9) is possible, but would further complicate the convergence of the numerical calculation with negligible impact on the final result. These expansions of density and velocity introduce significant numerical difficulty with four additional unknowns ($n_{j,k}^{c,s}$) in the numerical system of equations but its benefit of allowing more accurate calculation of rotation velocities and gyroviscosity is critical to the accuracy improvement over earlier studies [10–12]. Note that poloidal asymmetries in Eqs. (8) and (9) vary with radial position, but in order to simplify the calculation a separation of variables approximation is made, and for consistency the radial derivatives of these asymmetries are neglected during the development of the rotation calculation model [1].

In addition, it is implicitly assumed that the electron dynamics is determined by the ion dynamics via ambipolarity and neutrality constraints, but it is not necessary to assume anything about the electrons to calculate the ions because ion-impurity collisions are more important than ion–electron collisions so that the latter can be neglected.

2.2. Magnetic flux surface geometry

The geometry of the *D*-shaped elongated magnetic flux surface used in this study is given by Miller et al. [3] with elongation κ and triangularity δ as shown in Fig. 1. The R and Z coordinates of the Miller model are given by

$$R(r) = R_0(r) + r\cos(\theta + x\sin\theta) \equiv R_0(r) + r\cos\xi, \tag{10}$$

$$Z(r) = \kappa r \sin\theta, \tag{11}$$

where $R_0(r)$ is a function of r (the half-diameter from the center of plasma along the plasma mid-plane), $x \equiv \sin^{-1}\delta$, and $\xi \equiv \theta + x\sin\theta$.

Analysis of the curvilinear differential geometry in all coordinates (r, θ, ϕ) on the flux surfaces yields the following metric coefficients for the Miller geometry [3,16,17].

$$h_r = \frac{\kappa\left[\cos(x\sin\theta) + \frac{\partial R_0(r)}{\partial r}\cos\theta + \left[s_\kappa - s_\delta\cos\theta + (1+s_\kappa)\,x\cos\theta\right]\sin\theta\sin\xi\right]}{\sqrt{\sin^2\xi\,(1+x\cos\theta)^2 + \kappa^2\cos^2\theta}}, \tag{12}$$

$$h_\theta = \frac{r\kappa\left[\cos(x\sin\theta) + \frac{\partial R_0(r)}{\partial r}\cos\theta + \left[s_\kappa - s_\delta\cos\theta + (1+s_\kappa)\,x\cos\theta\right]\sin\theta\sin\xi\right]}{\sqrt{\left(\frac{\partial R_0}{\partial r} + \cos\xi - s_\delta\sin\xi\sin\theta\right)^2 + \kappa^2\sin^2\theta\,(s_\kappa+1)^2}}, \tag{13}$$

$$h_\phi = R(r) = R_0\,(1 + \varepsilon\cos\xi) \tag{14}$$

where $s_\kappa(r) = (r/\kappa)\,\partial\kappa/\partial r$ and $s_\delta(r) = r\,(\partial\delta/\partial r)\,/\sqrt{\left(1-\delta^2\right)}$ account for the radial changes in elongation and triangularity. Ampere's law provides the following magnetic field representations for the Miller model,

$$B_\theta(r,\theta) = \left(1 + \frac{\partial R_0(r)}{\partial r}\right)\frac{\overline{B}_\theta(r)}{h_r\,(1+\varepsilon\cos\xi)}, \tag{15}$$

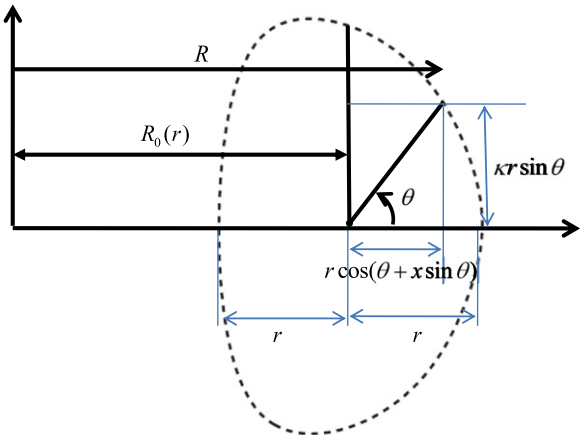

Fig. 1. Miller equilibrium flux surface geometry.

$$B_\phi = \frac{\overline{B}_\phi(r)}{1+\varepsilon\cos\xi}, \tag{16}$$

with the overbars indicating the values along the radial coordinate and the flux surface average (FSA) formula for this Miller geometry is given

$$\langle A(r,\theta)\rangle \equiv \frac{\oint \frac{A(r,\theta)d\ell_\theta}{B_\theta}}{\oint \frac{d\ell_\theta}{B_\theta}} = \frac{\oint A(r,\theta)Y(r,\theta)\,d\theta}{\oint Y(r,\theta)\,d\theta} \tag{17}$$

where

$$Y(r,\theta) = \frac{(1+\varepsilon\cos\xi)\left[\cos(x\sin\theta) + \frac{\partial R_0(r)}{\partial r}\cos\theta + [s_\kappa - s_\delta\cos\theta + (1+s_\kappa)x\cos\theta]\sin\theta\sin\xi\right]^2}{\sqrt{\left[\left(\frac{\partial R_0}{\partial r} + \cos\xi - s_\delta\sin\xi\sin\theta\right)^2 + \kappa^2\sin^2\theta\,(s_\kappa+1)^2\right]\left[\sin^2\xi\,(1+x\cos\theta)^2 + \kappa^2\cos^2\theta\right]}}. \tag{18}$$

2.3. Numerical calculation model

The extended neoclassical rotation equations [1] are developed by taking the flux surface average of the poloidal component of the momentum balance equation with 1, $\sin\theta$ and $\cos\theta$ as weighting functions and taking the flux surface average of the toroidal component of the momentum balance equation, for two ion species, and using the representation of Section 2.2. This procedure leads to eight equations in eight unknowns (4 velocities and 4 density asymmetries) at each radial location for a two-species plasma. Velocities and asymmetries are normalized to the same order of magnitude to avoid having equations of vastly different magnitudes by $\widehat{V}_{\theta j} \equiv \overline{V}_{\theta j}/\left(f_p V_{thj}\right)$, $\widehat{V}_{\phi j} \equiv \overline{V}_{\theta j}/V_{thj}$, and $\widetilde{n}_j^{c,s} \equiv n_j^{c,s}/\varepsilon$ where $f_p \equiv \overline{B}_\theta/\overline{B}_\phi$ and $\varepsilon \equiv r/R_0$.

In terms of the eight independent variables shown below,

$$\begin{aligned}
&\widehat{V}_{\phi i} = \widehat{V}_{\phi D} = \widehat{V}_{tD}: \text{ Toroidal Velocity (Deuterium)},\\
&\widehat{V}_{\phi I} = \widehat{V}_{\phi C} = \widehat{V}_{tC}: \text{ Toroidal Velocity (Carbon)}\\
&\widehat{V}_{\theta i} = \widehat{V}_{\theta D} = \widehat{V}_{pD}: \text{ Poloidal Velocity (Deuterium)},\\
&\widehat{V}_{\theta I} = \widehat{V}_{\theta C} = \widehat{V}_{pC}: \text{ Poloidal Velocity (Carbon)}\\
&\widetilde{n}_D^c = \widetilde{n}_i^c: \text{ Cos Asymmetry (Deuterium)},\\
&\widetilde{n}_C^c = \widetilde{n}_I^c: \text{ Cos Asymmetry (Carbon)}\\
&\widetilde{n}_D^s = \widetilde{n}_i^s: \text{ Sin Asymmetry (Deuterium)},\\
&\widetilde{n}_C^s = \widetilde{n}_I^s: \text{ Sin Asymmetry (Carbon)},
\end{aligned} \tag{19}$$

the resulting equations for the poloidal velocities and density asymmetries are of the form

$$A_{11}\widehat{V}_{\theta j}^2 + A_{12}\widehat{V}_{\theta j} + A_{13}\widehat{V}_{\theta k} = B_1 \tag{20}$$

$$A_{C1}\widetilde{n}_j^c + A_{C2}\widetilde{n}_j^s + A_{C3}\widetilde{n}_k^c = B_C \tag{21}$$

$$A_{S1}\widetilde{n}_j^c + A_{S2}\widetilde{n}_j^s + A_{S3}\widetilde{n}_k^s = B_S \tag{22}$$

with j being either i (deuterium) or I (carbon) and k being the other. Here $A_{11}, A_{12}, A_{13}, A_{C,S}, B_1$, and $B_{C,S}$ coefficients which depend on the other independent variables and are given in Appendix A. Eqs. (20)–(22) are the FSAs of Fourier moments of the poloidal momentum balance with all the terms retained, thus used to solve for the poloidal velocities and density asymmetries that are eventually coupled with

toroidal rotation computation model, which is developed by using the representation of Section 2.2 to evaluate the flux surface average of the toroidal momentum balance equation

$$\widehat{V}_{\phi i}\sqrt{m_I/m_i}\beta_i + \widehat{V}_{\phi I}\beta_I = (y_i + y_I)\,/V_{thI} \tag{23}$$

where $\beta_j \equiv \left(\nu_{dj} + \nu_{nj} + S_{nbj}/\overline{n}_j\right)/\left(\overline{\nu}_{jk} + \overline{\nu}_{je}\right)$ and $y_j = V_{thj}\left[\left(1+\beta_j\right)\widehat{V}_{\phi j} - \sqrt{m_j/m_k}\widehat{V}_{\phi k}\right]$ with ν_{nj} and ν_{dj} being the inertial and viscous transport frequencies respectively, and S_{nb} being neutral beam source, and

$$\widehat{V}_{\phi i} - \sqrt{\frac{m_i}{m_I}}\widehat{V}_{\phi I} = \left(\widehat{V}_{\theta i} - \sqrt{\frac{m_i}{m_I}}\widehat{V}_{\theta I}\right)\frac{\left\langle\frac{1}{1+\varepsilon\cos\xi}\right\rangle}{\left(1+\frac{\partial R_0(r)}{\partial r}\right)\left\langle\frac{1}{(1+\varepsilon\cos\xi)}\frac{1}{h_r}\right\rangle} + \left(-\widehat{P}_i + \sqrt{\frac{m_i}{m_I}}\widehat{P}_I\right)\frac{\left\langle\frac{1}{h_r}\right\rangle}{\left(1+\frac{\partial R_0(r)}{\partial r}\right)\left\langle\frac{1}{(1+\varepsilon\cos\xi)}\frac{1}{h_r}\right\rangle}. \tag{24}$$

Eqs. (20)–(24) constitute the extended neoclassical rotation model. Eqs. (23) and (24), which determine the toroidal rotation velocities, depend explicitly on the poloidal rotation velocities and implicitly on the poloidal density asymmetries which enter through the gyroviscous momentum transfer frequencies ν_{dj}. Eqs. (20)–(22), which determine the density asymmetries and the poloidal velocities, have coefficients which depend on the other independent variables. Therefore, most of the coefficients given in Appendix A are the functions of a combination of other independent variables, yielding a highly nonlinear coupled system of equations.

The quadratic term in Eq. (20) is treated iteratively

$$A_{11}\widehat{V}^n_{\theta j}\widehat{V}^{n-1}_{\theta j} + A_{12}\widehat{V}^n_{\theta j} + A_{13}\widehat{V}^n_{\theta k} = {B_1}^n \tag{25}$$

as a linear term with n being the current iteration step and $n-1$ being the previous step. With the quadratic equation possibly having two solutions, this iteration helps steer the algorithm towards the solution that is near the initial guesses of poloidal velocity.

2.4. Decomposition of computation model

The eight equations and eight unknowns in the previous section constitute a self-consistent 8-by-8 nonlinearly coupled numerical computation system. For this extremely ill-conditioned nonlinear system, various standard iterative techniques [4–6] such as Gauss–Seidel (G–S), SOR, and Newton's method have been tested to converge to a single solution with no success. Investigation of possible preconditionings of the coefficient matrices did not yield any promising improvement either. Thus, the first step we take to handle this ill-conditioned 8-by-8 system is to decompose it into three subsystems, as was previously done [9]. This decomposition, indicated in Eqs. (26)–(28), isolates the sources of ill-conditioning to the respective subsystems so that reformulation of each subsystem to improve its corresponding conditioning becomes much easier.

$$\text{Poloidal rotation subsystem: } \begin{bmatrix} c_{11} & c_{12} \\ c_{21} & c_{22} \end{bmatrix}\begin{bmatrix} \widehat{V}_{\theta i} \\ \widehat{V}_{\theta I} \end{bmatrix} = \begin{bmatrix} d_1 \\ d_2 \end{bmatrix}. \tag{26}$$

$$\text{Density asymmetry subsystem: } \begin{bmatrix} a_{11} & a_{12} & a_{13} & 0 \\ a_{21} & a_{22} & 0 & a_{24} \\ a_{31} & 0 & a_{33} & a_{34} \\ 0 & a_{42} & a_{43} & a_{44} \end{bmatrix}\begin{bmatrix} \widetilde{n}^c_i \\ \widetilde{n}^s_i \\ \widetilde{n}^c_I \\ \widetilde{n}^s_I \end{bmatrix} = \begin{bmatrix} b_1 \\ b_2 \\ b_3 \\ b_4 \end{bmatrix}. \tag{27}$$

$$\text{Toroidal rotation subsystem: } \begin{bmatrix} e_{11} & e_{12} \\ e_{21} & e_{22} \end{bmatrix}\begin{bmatrix} \widehat{V}_{\phi i} \\ \widehat{V}_{\phi I} \end{bmatrix} = \begin{bmatrix} f_1 \\ f_2 \end{bmatrix} \tag{28}$$

where all the coefficients are given in Appendix B. This decomposition into the separately iterated subsystems of Eqs. (26) and (27) significantly reduced the singularity effects relative to the combined system. However, there was little improvement on singularities in the toroidal subsystem of Eq. (28). Isolation of the singularity points in the final processing of the toroidal subsystem of Eq. (28) is possible based on our experience with DIII-D with NBI(Neutral Beam Injection) inputs that the radial profiles of rotation velocities vary smoothly so that dramatic discontinuities in the radial structure of the solution is indicative of numerical ill-conditioning, which can be easily checked against the conditioning number profiles of all subsystems in Eqs. (26)–(28). Noting that radial discontinuities can actually exist in tokamaks when poloidal velocity is in transonic range [18], comparison of the conditioning numbers and calculated velocities profiles will allow the identification of such discontinuities when poloidal velocities exceed poloidal sound speed. It is important to note that each mesh is iterated independently, thus has its own independent nonlinear dynamics although the dynamics of nearby meshes tend to be similar.

3. Numerical solution methodology

Now with the given decomposed numerical computation model in the previous section, there still remain two major numerical challenges. First is the instability of the nonlinear iteration dynamics and second is the identification of the true solution from the several feasible solutions generated by nonlinear iterations. In short, the former was successfully controlled with nonlinear SOR [4–6] and the latter accomplished by SA [7,8]. Before discussing the details of these methods, it is necessary to briefly discuss the differences in linear and nonlinear programming to understand the rationale for the methods used in this extended neoclassical rotation calculation.

3.1. Linear and nonlinear programming

Linear programming [4,19,20] is the study of maximizing or minimizing linear functions subject to linear equality and inequality constraints. Since linear functions are both convex and concave, any local minimum or maximum must be a global optimum. Thus, excepting

numerical issues, there is no issue with convergence to the "wrong" solution. Therefore, the literature [4,5,20,21] on linear programming only discusses how fast each algorithm can converge, and as long as storage is not a concern faster convergence is always preferred.

For simple and standard nonlinear problems [4,5,20,21], it is also possible to converge to a single solution using standard numerical methods such as Newton's method and its variants. In the nonlinear non-convex case [6,22,23], which includes many practical physics problems, the situation changes quite significantly. The higher the nonlinearity is, the higher the chance of failing to converge to the physical solution. In this case the iteration will often try to converge towards the true (physical) solution but will eventually be disturbed by numerical noise, then drive towards other solutions [6]. Keeping track of these various approximate solutions as the algorithm progresses, the algorithm generates several feasible solutions [21–23], corresponding to the local minima in nonlinear topological maps, but only one of them corresponds to the true physical solution. Then, a technique becomes necessary to identify the true solution from the nonlinear topological maps [8,22]. Considering that most minimization techniques [5,21] tend to converge to the nearest local minimum, application of the global minimum search concepts from SA [7,8] greatly reduces the risk of identifying a wrong solution as the true solution and allows searching for a global minimum within physically feasible range.

Another issue is the importance of the accuracy of initial guesses for any iterative programming [4,5,21,23]. When the initial guesses are too far from the true solution, even simple linear and nonlinear problems can continue diverging the iterations far from the true solution, increasing the risk of identifying a wrong solution as the true solution even if it converges. With nonlinear physics problems, the accuracy of initial guesses becomes increasingly important because a minimization algorithm will eventually search for the solution near the initial guesses [4,5], but SA gives the algorithm greater flexibility by allowing it to test all the feasible solutions within the feasible range [7,8]. For the extended rotation calculation in this paper [1], the initial guesses for the velocities are believed to be very accurate because the initial $\widehat{V}_{\theta I}$ and $\widehat{V}_{\phi I}$ for the impurity (carbon) come directly from experimental measurement, and the initial deuterium $\widehat{V}_{\phi i}$ is inferred from perturbation theory [24] with $\widehat{V}_{\phi I}$ as an input, and the initial deuterium $\widehat{V}_{\theta i}$ is calculated with other initial guesses based on the momentum balance equation. The initial guesses for $\widetilde{n}_j^{c,s}$, however, can be neither measured nor inferred, thus zeros are used. We note that it is the nature of nonlinear equations such as those are solved here to have various "local minima" in the phase space of unknowns. We have found that when we start with good initial guesses then we obtain solutions in good agreement with experimental measurements, but that poor initial guesses sometimes converge to other, non-physical, which emphasizes the importance of good initial guesses and the need for procedures to distinguish between the physical solution and non-physical local minima.

In terms of the dynamics of the numerical system, nonlinear algorithms are vulnerable to instability (i.e., high sensitivity to numerical errors) [6,23]. Since all nonlinear problems must be solved iteratively, there are several factors that affect the dynamics of the iterations such as conditioning of the system, degree of nonlinearity, characteristics of the chosen numerical method, accuracy of the initial guesses, etc. Instability of the system dynamics was surely an issue for the extended neoclassical rotation calculation, especially with the ill-conditioned toroidal rotation subsystem in Eq. (28). Fortunately, under-relaxation worked very effectively, making nonlinear SOR with optimal relaxation weight the key to the stable iterative dynamics of the given problem [1]. This dependence of the dynamic stability on many factors also implies that the final solutions may also slightly vary within a stable range depending on the chosen algorithm, relaxation scheme, etc. [23,25].

3.2. Nonlinear SOR method and instability control

Fig. 2 is a flowsheet for the nonlinear SOR algorithm for the extended neoclassical rotation calculation model. Since the initial guesses for $\widetilde{n}_j^{c,s}$ are zeros, these are allowed to be updated whenever new $\widehat{V}_{\phi,\theta}$ values are available. Testing the algorithm with final calculated asymmetries as new initial guesses appears to help stabilize iteration dynamics of the system, but is left for future investigation as a longer run-time and manual input of new asymmetries are not desirable for a user-friendly code.

Theoretically, there exists an optimal relaxation set of weights when solving minimization problems with iterative SOR [4,5,21]. The extended rotation calculation model in this paper [1] adaptively determines the relaxation weights (w) based on the conditioning of the subsystems at initial iteration ($n = 1$) by

$$w = \frac{\alpha}{\mathrm{cond}(A)^{n=1}}. \tag{29}$$

Here α is a constant fixed for all 51 meshes, usually $0.2 \le \alpha \le 2$, and $\mathrm{cond}(A)^{n=1}$ is the condition number of each mesh in Eqs. (26) and (28) at the initial step, usually $3 < \mathrm{cond}(A) < 100$ except for the near singularity meshes (high condition numbers) shown in Fig. 3. With the normalized distance $\rho(\mathrm{rho}) \equiv r/a$ where a is the maximum radius along r coordinate of the plasma column, Fig. 3 shows an example of the extreme ill-conditioning of the toroidal rotation subsystem near $\rho = 0.25$, $\rho = 0.67$, $\rho = 0.84$, and in the plasma edge, which are introduced by one of the coefficients (e_{11}) in Eq. (28) crossing zero axis at the corresponding meshes.

In dealing with the unstable iterative dynamics of this ill-conditioned system, the adaptive weight scheme in Eq. (29) serves two purposes: (i) the relaxation weight is smaller when the conditioning is worse at a near singular mesh, giving all the meshes the same order of deviation magnitude while iterations continue; and (ii) it prevents a premature termination of the algorithm when a calculated value at a singular mesh reaches OFL (OverFlow Level) due to high numerical sensitivity. Premature termination needs to be avoided so that the algorithm can generate topological maps with enough feasible solutions(at least three, empirically) for SA to test them for the true solution. Thus, for the rotation subsystems in Eqs. (26) and (28), the new output velocities at nth iteration are calculated by

$$\widehat{V}^n(\mathrm{new}) = (1 - w)\ \widehat{V}^{n-1} + w\,\widehat{V}^n(\mathrm{old}). \tag{30}$$

3.3. Nonlinear topological maps and simulated annealing

Nonlinear topological maps can be drawn with many iterative parameters but most commonly by "relative" residuals (or errors) computed with either $\|r_n\| / \|r_1\|$ or $\|r_n\| / \|r_{n-1}\|$ where r_n is the residual at nth iteration, r_{n-1} is at the previous step iteration, and r_1 is at

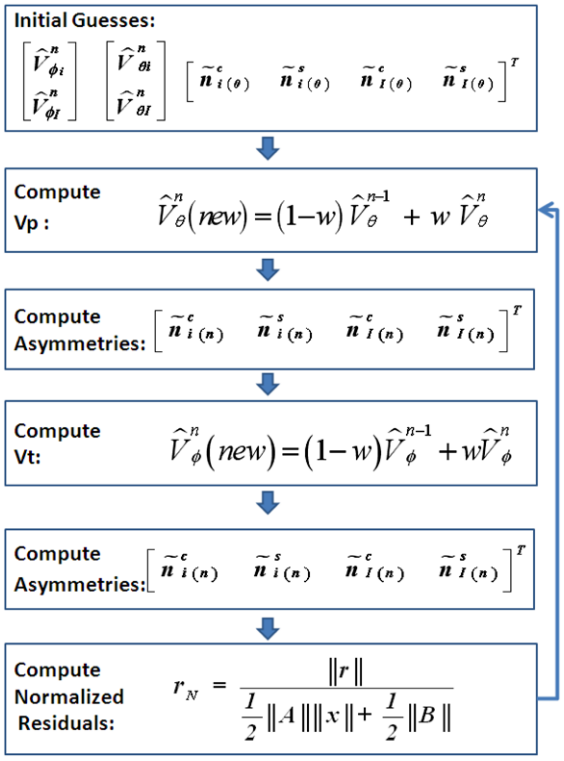

Fig. 2. SOR flowsheet.

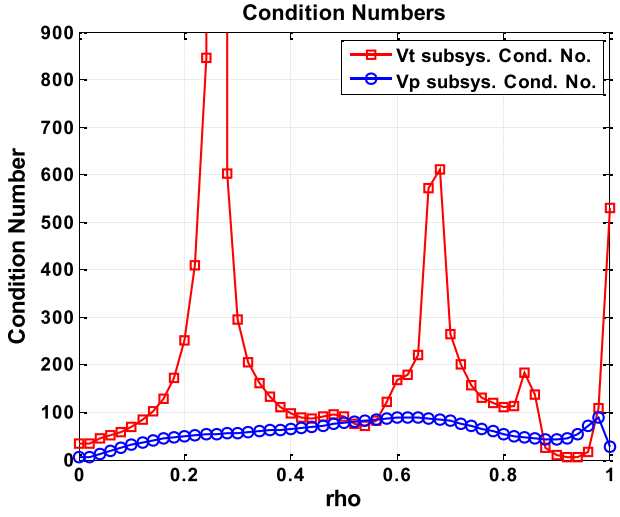

Fig. 3. Condition numbers at initial iteration step.

the initial iteration [4–6]. Application of these popular relative residuals yields noisy topological maps probably because the coefficients on both sides of each subsystem constantly change its relative magnitudes, especially with the initial guesses of $\widetilde{n}_j^{c,s}$ being zeros. To measure the error magnitude relative to the size of constantly-changing subsystems, a new concept called "normalized" residual (r_N) at the nth iteration step given by

$$r_N{}^n \equiv \frac{\|r^n\|}{\frac{1}{2}\|A^n\|\,\|x^n\| + \frac{1}{2}\|b^n\|} \tag{31}$$

is devised for a general nth iteration system, $A^n x^n = b^n$, where $r^n = b^n - A^n x^n$ is its residual. This normalized residual allows a heuristic measure of the residual size relative to the magnitude of each iteration system. For example, $r_N{}^n = 10^{-3}$ indicates that the residual is one thousandth when the entire system magnitude is normalized to one. Since r_N is calculated for both poloidal and toroidal subsystems, topological maps for the entire system dynamics are given by the 2-norms of both normalized residuals of Eqs. (26) and (28) as shown in Figs. 4 and 5.

With topological maps provided, a simple local minima searching algorithm can assist SA to identify a global minimum within the feasible range, eliminating the need of applying a complete implementation of SA [7]. From the empirical testing of the nonlinear dynamics

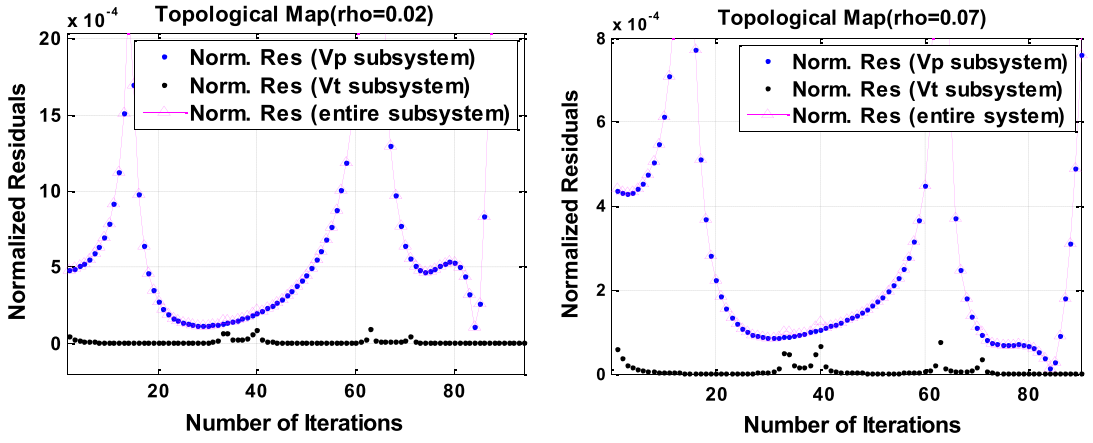

Fig. 4. Topological maps for the meshes for $\rho < 0.25$ ($\alpha = 0.5$).

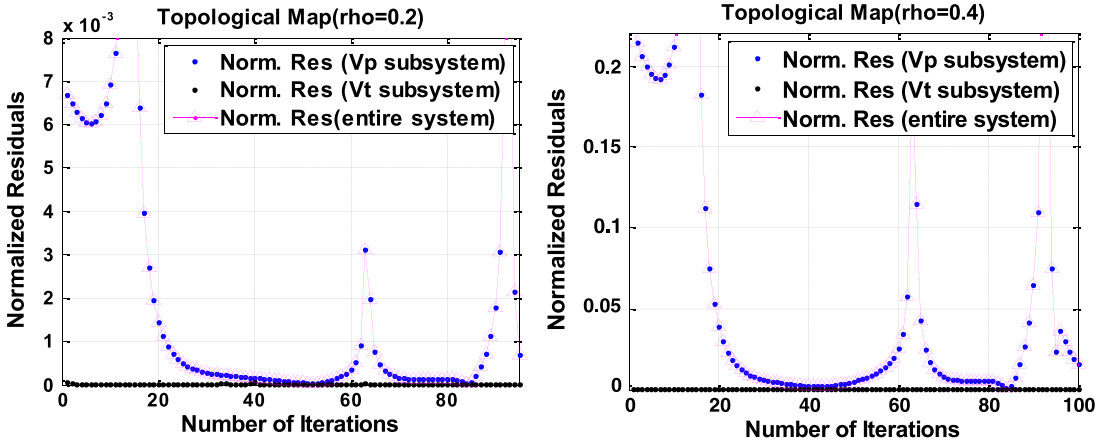

Fig. 5. Topological maps for the meshes for $\rho > 0.25$ ($\alpha = 0.5$).

of the given problem in this paper, there are two important considerations when applying SA. First, it is practically efficient to set a physically feasible range and locate a "locally" global minimum within that range. This is also a good practice when we know that the initial guesses are quite close to the true solution as is the case with the given problem. Second, understanding that nonlinear algorithms with high numerical sensitivity tend to eventually drive the iterations to trivial solutions [6,25], all feasible solutions need to be tested for trivial solutions because these are usually identified with much smaller normalized residuals than those of the true solution. In the plasma rotation calculation with strong beam injection, any solution(s) with zero velocity (or velocities) can be considered trivial solution(s). Therefore, the use of SA within local (not global) feasible range and elimination of trivial solutions based on physics argument are empirically proven to be the best minimization method for the extended neoclassical rotation calculations [1].

3.4. Nonlinear dynamics of the extended neoclassical rotation model

Using the numerical methodology discussed in the previous section, the extended neoclassical rotation calculation algorithm was applied to two DIII-D discharges and the following summarizes the observed characteristics of the nonlinear iterative dynamics of the given problem [1]. First, the iteration has strong tendency to drive towards trivial solutions especially with larger w values (i.e., larger α). This means that with w too large it is possible for the true solution to turn into a saddle point, thus not be presented as one of the feasible solutions. With w too small, the algorithm generates too many feasible solutions, all of which except one are transient solutions. To assist identification of the true solution, the algorithm can be tested to run with the measured velocities (VtC) fixed and generate converged solution for corresponding poloidal velocities. Then with the identified poloidal velocities, α value can be adjusted to its optimal value to generate corresponding true solution set with all eight unknowns. Relaxation scheme in Eqs. (29) and (30) worked well for the two DIII-D shots analyzed [1]. Though only two shots were tested, unique characteristics of each shot allowed a sufficient degree of generalization with differences in flux surface geometry (upper vs. lower null divertor) and in torque injection direction relative to the plasma current. Details on two DIII-D shots used during the development of the algorithm are provided in Ref. [1]. More analysis of different shots will be done in the near future to categorize types of shots based on the shot characteristics and their respective dynamic responses but the main relaxation scheme in Eqs. (29) and (30) is expected to stay the same.

Secondly, certain relaxation weights, supposedly very close to the optimal α, allow the system to stagnate near the true solution. With optimal α value, it appears that the algorithm tries to converge to a stagnant solution, increasing the confidence when it agrees with the converged poloidal velocities with VtC fixed at measured values and with the true solution selected by SA, which is the case for two shots

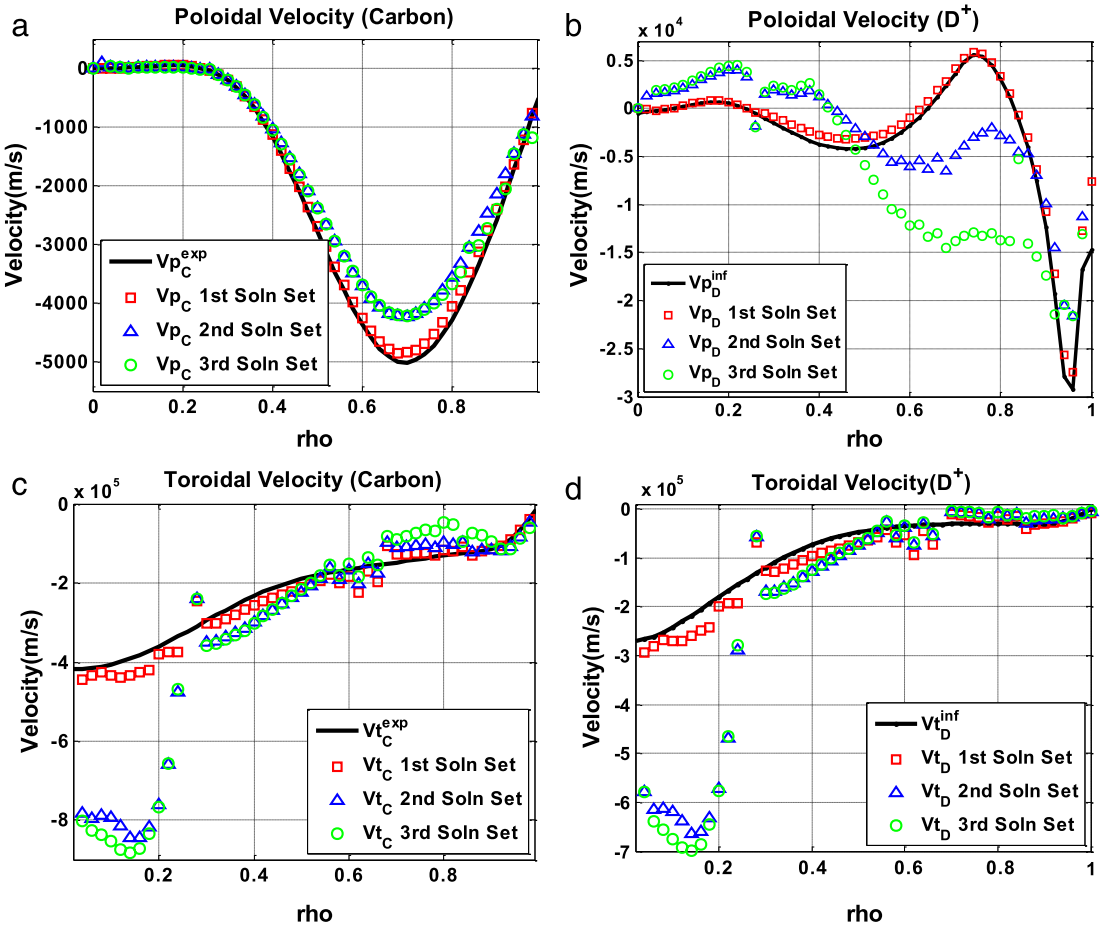

Fig. 6. Feasible solution sets for local minima in Figs. 4 and 5 (toroidal velocities: CW positive/poloidal velocities: positive upward at outer mid-plane).

in this study [1]. Lastly, the true solutions are usually identified with $r_N{}^n$ below 10^{-3} before getting disturbed again by numerical noises. Analysis on more shots are required to generalize this finding but with the trivial solutions usually yielding $r_N{}^n$ lower by more than an order of magnitude (below 10^{-4}) it can be used as a criterion to test any local minimum for the true solution in future algorithms.

4. Application of simulated annealing

Out of the two shots analyzed with a combination of nonlinear SOR and SA [1], one of them contains a good mix of the characteristics discussed in the previous section with more stable dynamics, thus we focus our discussion on this shot. Figs. 4 and 5 present topological maps for the four selected mesh points for this shot with $\alpha = 0.5$. The first three local minima in these maps correspond to the three feasible solutions in Fig. 6.

There are subtle differences between the topological maps in Figs. 4 and 5 because the iterative dynamics are different from the mesh points on the left and right side of $\rho = 0.25$. The iterative dynamics of the mesh points in $0.25 < \rho < 1$ range, with their sample topological maps in Fig. 5, are more stable because the 2nd and 3rd solution sets in Fig. 6 for the well-conditioned mesh points stay quite closer to each other (i.e., stagnate at these solutions) for about up to 40 iterations except the deuterium poloidal velocity in Fig. 6(b), possibly indicating that the algorithm may converge the iterations to these solutions unless disturbed by the numerical noises. With all three solutions being possible candidates for the true solution in this range, SA identifies the 2nd solution set with the lowest $r_N{}^n$ as the true solutions. On the other hand, the mesh points on the left side of $\rho = 0.25$ in Fig. 6, with their sample topological maps in Fig. 4, are driven towards the trivial solutions much faster because according to Eq. (29) this region has much higher w values. $V_{\theta I}$ values in this range quickly drive to zeros and introduce numerical errors in other velocities causing them to jump to much higher values, which is a typically observed response of the system at trivial solutions. Therefore, in this range the first solution set with $r_N{}^n$ well below 10^{-3} corresponds to the true physical solution and it can be verified with lower α values to yield the same type of iterative dynamics as in $0.25 < \rho < 1$ range. It was also checked that VpC in Fig. 6(a) corresponds to the converged solution with VtC fixed at measured values.

Comparing Fig. 6(c) and (d) with the condition number profiles of the same shot in Fig. 3, it can be observed that the mesh points with near singularity are highly sensitive to numerical round-off errors. The present algorithm simply neglects these near singular meshes from the output and spline connects the entire radial profile based on the physics argument that DIII-D shots with NBI inputs have smooth radial rotation profiles. Thus, Fig. 7 shows the final processed velocity profiles along with the initial guesses for the chosen shot. Note that the toroidal velocities are shown as positive counter-clockwise (CCW) to indicate in the direction of the neutral beam injection (in the notation used to describe rotation in DIII-D, the rotation would be negative). Fig. 8 shows the final non-normalized density asymmetries ($n_j^{c,s}$), which

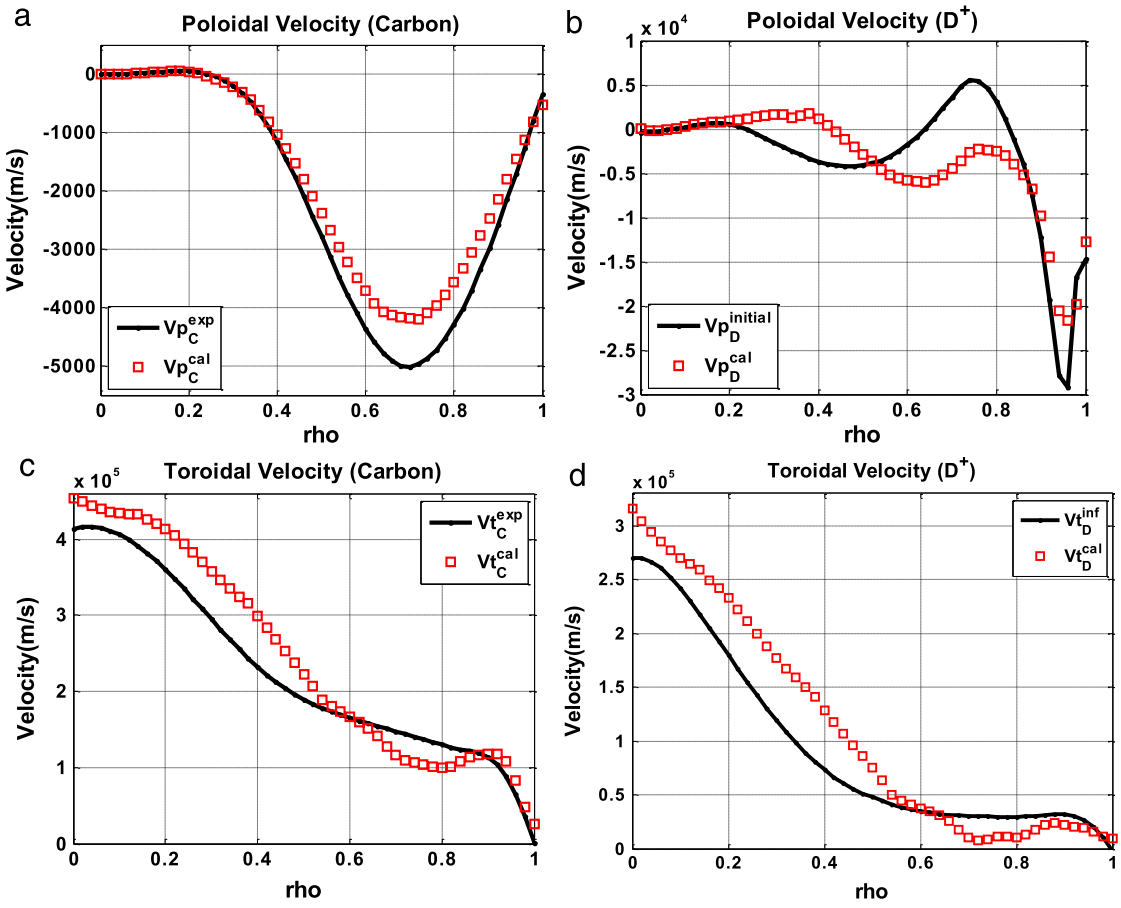

Fig. 7. Final true solution velocity profiles (toroidal velocities: CCW positive/poloidal velocities: positive upward at outer mid-plane).

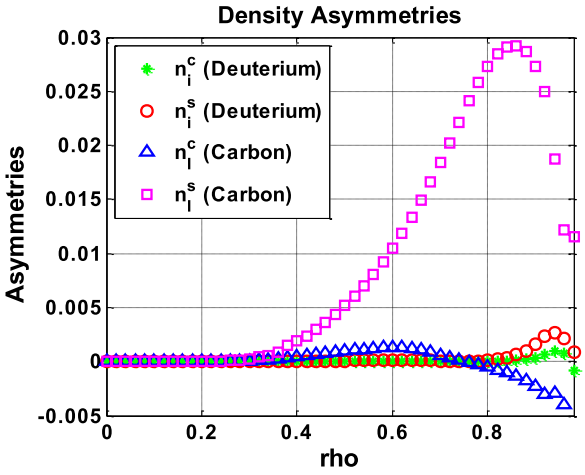

Fig. 8. Computed density asymmetries.

are the additional variables that made this extended neoclassical calculation model highly nonlinear. Note that velocity asymmetries $V_j^{c,s}$ can be computed from these $n_j^{c,s}$ since they are related through the momentum balance and continuity equations (see Appendix A for the relations).

5. Verification of the algorithm and of the results

Currently the most robust way to check the validity of the true solution identified through SA is to test the algorithm with fixed VtC at its measured values (i.e., applying the same SOR algorithm with seven unknowns) and check that the true solution identified with all eight unknowns corresponds with the local minimum of the converged poloidal velocities. This test of the true solution with VtC fixed is

expected to be provided as an option in the future version of GTROTA. Another rigorous verification was done during the code development phase by turning off some variables (i.e., fixed them at initial guesses) selectively with different combinations of variables to check the solutions against known characteristics of simpler plasma rotation models [9–12]. In the simplest case, with the asymmetry and toroidal velocities fixed at their initial guesses, the algorithm can be checked to generate the same solutions as in solving a simple linear poloidal rotation subsystem in Eq. (26). Then, turning on the toroidal velocity subsystem in Eq. (28) allows nonlinear calculation of the velocities with no asymmetries ($\widetilde{n}_j^{c,s} = 0$), which we would predict to be less accurate poloidal velocities that eventually translate into the over-prediction of toroidal velocities [26]. Finally, turning on the asymmetry iterations of Eq. (27), we can observe the evolution of the true physical solutions to our final solutions in Fig. 7.

Comparison of GTROTA against other numerical codes such as NCLASS [10] or NEO is not performed during the development of the code but left as future exercise. Direct comparison with each code or theory is somewhat difficult because NCLASS does not calculate poloidal asymmetries and hence does not evaluate gyroviscosity, and the NCLASS calculation of perpendicular viscosity is much too small to explain the toroidal rotation damping. Hinton–Wong [27] assume that the up–down poloidal asymmetries vanish, hence effectively assume that the gyroviscosity is zero. Direct comparison may be possible if these codes or theories are extended to include gyroviscosity and poloidal asymmetries in their formalism. For the two cases [1] analyzed with the current code significantly improved agreement of the calculated carbon velocities (VtC and VpC) against the measured values and against earlier extended theory based on circular flux surface geometry [9] is the verification of improvement over other codes.

6. Future research

The next theoretical research directions for the extended neoclassical rotation theory [1] are the extension of the current theory to include (i) the divertor X-point dependence of the magnetic flux surfaces, (ii) Mikhailovskii–Tsypin's weak rotation ordering viscosity tensor [28–31], and (iii) the charge-exchange of recycling neutrals, all of which would increase the accuracy in the plasma edge and extend applicability to plasmas with weak rotation. The Miller model flux surface geometry could certainly be extended to provide a more realistic representation of the X-point elongation.

In terms of numerical analysis, however, the same challenges are expected since the nonlinear dynamics would be very similar to the ones presented in this paper. To improve the current algorithm in future studies, there are some possible candidate approaches in addition to the minor upgrades suggested in earlier sections. First, realizing that the practical physics problems can be formulated into numerical calculation models in a variety of ways, examination of other decompositions of the subsystems in Eqs. (26)–(28) to eliminate singularities and efforts to improve conditioning of the coefficient matrices by separating singularity-causing subterms of diagonal components in the matrices to the right-hand side of the equations are being investigated. The singular meshes were identified as the main source of numerical noises because they migrate to near-by meshes as iterations continue. More analyses of other shots are expected to help identify common diagonal subterms that cause singularities and decomposed subsystems with these singularity-causing subterms handed over to the right-hand side may be offered as optional solution algorithm in the future code.

Another aggressive restructuring of the problem by identifying new additional relations to set up the entire problem as a least squares problem has gone through some initial investigation, showing improvements with conditioning of the toroidal rotation subsystem, but this approach requires significant further investigation. Another future effort would be in extending the capability of the current algorithm to handle problems with a diverse combination of inputs, especially ones with no VpC measurements, because tokamak experiments and diagnostics are focused on different discharge parameters with different accuracy level. To analyze shots with substantially different parameters, the current numerical algorithm of this paper may need to be modified. Therefore, along with a future theoretical research on the extended neoclassical rotations, efforts on the improvement of the corresponding numerical model and methodology should continue as well.

7. Conclusions

The extended neoclassical rotation equations [1] for tokamak plasmas, which provide a better representation of the poloidal dependence of the elongated magnetic flux surface geometry, make the resultant numerical computation model highly nonlinear. Direct iteration of the coupled equations to a converged solution was found to be practically impossible except with reduced number of unknowns. A decomposition of the governing equations into subsystems of equations, Eqs. (26)–(28), that are separately iterated to convergence within an overall iteration has been developed and implemented to solve the new nonlinear set of tokamak neoclassical rotation equations [1]. Based upon a study of the nonlinear dynamics of the given minimization problem, an algorithm combining the nonlinear SOR and SA is found to be the most reliable and effective method. For the application of SA, the feasible range is determined based on reasonable physics arguments to eliminate trivial solutions (zero velocities), and the search for the "locally" global minimum is made within this range. In the absence of known solutions for this type of nonlinear problem, the results are verified by testing the algorithm with intermediate solutions with a reduced number of variables and also by using a wide range of relaxation weights, thus increasing the robustness of the algorithm and the results.

The numerical scheme used in the current code is generalized for two shots [1] but the main solution methodology is expected to stay the same. Application to more shots with diverse cases will help further generalize the algorithm and provide more options to allow checks on the true solution while minimizing numerical noises, thus yielding more user-friendly code in the near future.

Acknowledgments

The authors are grateful to Dr. Wayne M. Solomon at PPPL for his TRANSP inputs during the development and testing of the code. This work was supported by the US Department of Energy under grant DE-FG02-ER54538 with the Georgia Tech Research Corporation.

Appendix A. Coefficients in the extended neoclassical rotation equations

A.1. Poloidal momentum balance equation (1 moment)

$$A_{11} = qrf_p^2\widetilde{n}_j^s\left(\left\langle\frac{\cos\theta}{h_\theta}\right\rangle + \frac{\left\langle\frac{1}{R}\frac{\partial R}{\partial\theta}\frac{\sin\theta}{h_\theta}\right\rangle}{\left\langle\frac{\sin^2\theta}{h_\theta}\right\rangle}\left\langle\frac{\cos^2\theta}{h_\theta}\right\rangle\right),$$

$$\begin{aligned}A_{12} \;=\; &\left[-q^2{R_0}^2f_pf_j\left\{\widetilde{n}_j^c\varepsilon\left[-\frac{1}{3}\frac{\left\langle\frac{1}{R}\frac{\partial R}{\partial\theta}\sin\theta\frac{1}{h_\theta}\right\rangle}{\left\langle\frac{\sin^2\theta}{h_\theta}\right\rangle}\left(\left\langle\frac{\sin^2\theta}{(h_\theta)^2}\right\rangle-\left\langle\frac{\cos^2\theta}{(h_\theta)^2}\right\rangle\right)+\frac{1}{3}\left\langle\frac{\partial h_\theta}{\partial\theta}\frac{\sin\theta}{(h_\theta)^3}\right\rangle\right.\right.\\
&\left.-\left\langle\frac{1}{R}\frac{\partial R}{\partial\theta}\frac{\sin\theta}{(h_\theta)^2}\right\rangle-\frac{1}{3}\left\langle\frac{\cos\theta}{(h_\theta)^2}\right\rangle\right]+3\langle Q\rangle+\langle M\rangle\\
&+\frac{\left\langle\frac{1}{R}\frac{\partial R}{\partial\theta}\sin\theta\frac{1}{h_\theta}\right\rangle}{\left\langle\frac{\sin^2\theta}{h_\theta}\right\rangle}\left(-\frac{1}{3}\left\langle\frac{\partial h_\theta}{\partial\theta}\frac{\sin\theta}{(h_\theta)^3}\right\rangle+\left\langle\frac{1}{R}\frac{\partial R}{\partial\theta}\frac{\sin\theta}{(h_\theta)^2}\right\rangle+\frac{1}{3}\left\langle\frac{\cos\theta}{(h_\theta)^2}\right\rangle+\langle M\cos\theta\rangle-\langle P\sin\theta\rangle\right)\Bigg\}\\
&\left.+\left(qrf_p\widehat{V}_{\phi j}\widetilde{V}_\phi^s\left\langle\frac{1}{R}\frac{\partial R}{\partial\theta}\frac{\sin\theta}{h_\theta}\right\rangle-f_p\sum_{j\neq k}\overline{\nu}_{jk}^*-f_p\nu_{\mathrm{atom}j}^*\right)\right],\end{aligned}$$

$$A_{13} = f_p\sum_{j\neq k}\overline{\nu}_{jk}^*\sqrt{\frac{m_j}{m_k}},$$

$$\begin{aligned}B_1 \;=\; &\widehat{V}_{\phi j}\widetilde{V}_{\phi j}^c q^2{R_0}^2f_jf_p\varepsilon\left(\left\langle\frac{\partial h_\theta}{\partial\theta}\frac{\sin\theta}{(h_\theta)^3}\right\rangle-\left\langle\frac{\cos\theta}{(h_\theta)^2}\right\rangle-\langle N\cos\theta\rangle-2\left\langle\frac{1}{R}\frac{\partial R}{\partial\theta}\frac{\sin\theta}{(h_\theta)^2}\right\rangle\right)\\
&+\widehat{V}_{\phi j}q^2{R_0}^2f_jf_p\left[\varepsilon\widetilde{n}_j^c\left(\left\langle\frac{1}{R}\frac{\partial R}{\partial\theta}\sin\theta\frac{1}{(h_\theta)^2}\right\rangle-\langle N\cos\theta\rangle\right)-\langle N\rangle-3\left\langle\left(\frac{1}{R}\frac{\partial R}{\partial\theta}\right)^2\frac{1}{(h_\theta)^2}\right\rangle\right]+\frac{1}{2}qr\widetilde{n}_j^s\left\langle\frac{\cos\theta}{h_\theta}\right\rangle\\
&-\left\langle M_{\theta j}\right\rangle\frac{qR_0}{\overline{n}_jm_jV_{thj}^2}+\widehat{V}_{rj}\left\langle\frac{1}{(1+\varepsilon\cos\xi)}\right\rangle+\frac{1}{2}qr\varepsilon\overline{\overline{\Phi}}_j\left[\widetilde{\Phi}^s\left(\frac{1}{\varepsilon}\left\langle\frac{\cos\theta}{h_\theta}\right\rangle+\widetilde{n}_j^c\left\langle\frac{\cos^2\theta}{h_\theta}\right\rangle\right)-\widetilde{n}_j^s\widetilde{\Phi}^c\left\langle\frac{\sin^2\theta}{h_\theta}\right\rangle\right]\end{aligned}\tag{A.1}$$

where q is safety factor, M_θ is poloidal momentum input, $f_p \equiv \overline{B}_\theta/\overline{B}_\phi$, $\nu_{\mathrm{atom}j}^* \equiv \frac{qR_0}{V_{thj}}\overline{\nu}_{\mathrm{atom}j}$, $\widehat{V}_{rj} \equiv \frac{qR_0e_j\overline{B}_\phi}{m_jV_{thj}^2}\overline{V}_{rj}$, $\overline{\overline{\Phi}}_j \equiv \frac{e_j\overline{\Phi}}{1/2\,m_jV_{thj}^2} = \frac{e_j\overline{\Phi}}{T_j} = \frac{Z_je\overline{\Phi}}{T_j}$, $\overline{\nu}_{jk}^* \equiv \frac{qR_0}{V_{thj}}\overline{\nu}_{jk}$, $f_j \equiv \frac{\varepsilon^{-3/2}\nu_{jj}^*}{\left(1+\varepsilon^{-3/2}\nu_{jj}^*\right)\left(1+\nu_{jj}^*\right)}\widehat{\Phi}_j' = \frac{\overline{\Phi}'}{V_{thj}} \equiv \frac{1}{V_{thj}\overline{B}_\theta}\frac{\partial\overline{\Phi}}{\partial r} = -\frac{\overline{E}_r}{V_{thj}\overline{B}_\theta}$, $\nu_{jj}^* \equiv \frac{\nu_{jj}qR_0}{V_{thj}} = \frac{qR_0}{V_{thj}\tau_{jj}}$, $\widetilde{\Phi}^{c,c} \approx \frac{T_e\widetilde{n}_e^{c,s}}{\overline{\Phi}e}$, $N \equiv -\left(\frac{1}{R}\frac{\partial R}{\partial\theta}\right)^2\frac{1}{(h_\theta)^2} - \frac{\partial h_\theta}{\partial\theta}\frac{1}{R}\frac{\partial R}{\partial\theta}\frac{1}{(h_\theta)^3} + \frac{1}{R}\frac{\partial^2R}{\partial\theta^2}\frac{1}{(h_\theta)^2}$, $M \equiv N + \frac{1}{3}\left[-\left(\frac{1}{B_\theta}\frac{\partial B_\theta}{\partial\theta}\right)^2\frac{1}{(h_\theta)^2} - \frac{\partial h_\theta}{\partial\theta}\frac{1}{B_\theta}\frac{\partial B_\theta}{\partial\theta}\frac{1}{(h_\theta)^3} + \frac{1}{B_\theta}\frac{\partial^2B_\theta}{\partial\theta^2}\frac{1}{(h_\theta)^2}\right]$, $P \equiv \frac{1}{R}\frac{\partial R}{\partial\theta}\frac{1}{(h_\theta)^2} + \frac{1}{3}\frac{1}{B_\theta}\frac{\partial B_\theta}{\partial\theta}\frac{1}{(h_\theta)^2}$, $Q \equiv \left(\frac{1}{R}\frac{\partial R}{\partial\theta}\right)^2\frac{1}{(h_\theta)^2} + \frac{1}{3}\left(\frac{1}{R}\frac{\partial R}{\partial\theta}\right)\left(\frac{1}{B_\theta}\frac{\partial B_\theta}{\partial\theta}\right)\frac{1}{(h_\theta)^2}$ with $\overline{\Phi}$ being the average electric potential.

A.2. Poloidal momentum balance equation (cosine moment)

$$A_{C1} = q^2R_0rf_jf_p\left[-\widehat{V}_{\theta j}\frac{1}{3}\left(-\left\langle\frac{\partial h_\theta}{\partial\theta}\frac{\sin\theta\cos\theta}{(h_\theta)^3}\right\rangle+\left\langle\frac{\cos^2\theta}{(h_\theta)^2}\right\rangle\right)-\widehat{V}_{\phi j}\left\langle N\cos^2\theta\right\rangle-\sum_{j\neq k}\overline{\nu}_{jk}^*\varepsilon f_p\sqrt{\frac{m_j}{m_k}}\widehat{V}_{\theta k}\left\langle\cos^2\theta\right\rangle-\widehat{V}_{rj}\varepsilon\left\langle\frac{\cos^2\theta}{(1+\varepsilon\cos\xi)}\right\rangle\right],$$

$$A_{C2} = qr\left(-f_p^2\widehat{V}_{\theta j}^2\left\langle\cos^2\theta\frac{1}{h_\theta}\right\rangle+\frac{1}{2}\left\langle\frac{\cos^2\theta}{h_\theta}\right\rangle\right),$$

$$A_{C3} = \sum_{j\neq k}\overline{\nu}_{jk}^*\varepsilon f_p\widehat{V}_{\theta j}\left\langle\cos^2\theta\right\rangle,$$

$$\begin{aligned}B_C = \;&qrf_p\widehat{V}_{\theta j}\widehat{V}_{\phi j}\widetilde{V}_\phi^s\left\langle\frac{1}{R}\frac{\partial R}{\partial\theta}\sin\theta\cos\theta\frac{1}{h_\theta}\right\rangle-\widehat{V}_{\theta j}q^2{R_0}^2f_jf_p\left[\frac{\left\langle\frac{1}{R}\frac{\partial R}{\partial\theta}\frac{\sin\theta}{h_\theta}\right\rangle}{\left\langle\frac{\sin^2\theta}{h_\theta}\right\rangle}\left(-\frac{1}{3}\left\langle\frac{\partial h_\theta}{\partial\theta}\frac{\sin\theta\cos\theta}{(h_\theta)^3}\right\rangle+\frac{1}{3}\left\langle\frac{\cos^2\theta}{(h_\theta)^2}\right\rangle\right.\right.\\
&\left.\left.+\left\langle M\cos^2\theta\right\rangle-\langle P\sin\theta\cos\theta\rangle\right)+\langle M\cos\theta\rangle+3\langle Q\cos\theta\rangle\right]\\
&-\widehat{V}_{\phi j}\widetilde{V}_{\phi j}^cq^2R_0rf_jf_p\left(\left\langle\frac{\partial h_\theta}{\partial\theta}\frac{\sin\theta\cos\theta}{(h_\theta)^3}\right\rangle-\left\langle\frac{\cos^2\theta}{(h_\theta)^2}\right\rangle-\left\langle N\cos^2\theta\right\rangle\right)-\widehat{V}_{\phi j}q^2{R_0}^2f_jf_p\left\langle N\cos\theta\right\rangle+\left\langle\cos\theta M_{\theta j}\right\rangle\end{aligned}$$

$$\times \frac{qR_0}{\overline{n}_j m_j V_{thj}^2} - \sum_{j\neq k} \overline{\nu}_{jk}^* f_p \left(\widehat{V}_{\theta j} - \sqrt{\frac{m_j}{m_k}}\widehat{V}_{\theta k}\right)\left(\langle\cos\theta\rangle + \frac{\left\langle \frac{1}{R}\frac{\partial R}{\partial\theta}\frac{\sin\theta}{h_\theta}\right\rangle}{\left\langle\frac{\sin^2\theta}{h_\theta}\right\rangle}\langle\cos^2\theta\rangle\right)$$

$$-\widehat{V}_{rj}\left\langle\frac{\cos\theta}{(1+\varepsilon\cos\xi)}\right\rangle - \frac{1}{2}qr\overline{\overline{\Phi}}_j\widetilde{\Phi}^s\left\langle\frac{\cos^2\theta}{h_\theta}\right\rangle - f_p\nu_{\mathrm{atom}j}^*\widehat{V}_{\theta j}\left(\langle\cos\theta\rangle + \frac{\left\langle \frac{1}{R}\frac{\partial R}{\partial\theta}\frac{\sin\theta}{h_\theta}\right\rangle}{\left\langle\frac{\sin^2\theta}{h_\theta}\right\rangle}\langle\cos^2\theta\rangle\right) \tag{A.2}$$

where $\widetilde{V}_\phi^{c,s}$ given in Eqs. (A.4) and (A.5).

A.3. Poloidal momentum balance equation (sine moment)

$$A_{S1} = qrf_p^2\widehat{V}_{\theta j}^2\left\langle\sin^2\theta\frac{1}{h_\theta}\right\rangle - \frac{1}{2}qr\left\langle\frac{\sin^2\theta}{h_\theta}\right\rangle,$$

$$A_{S2} = q^2R_0rf_jf_p\left[-\widehat{V}_{\theta j}\frac{1}{3}\left(\left\langle\frac{\partial h_\theta}{\partial\theta}\frac{\sin\theta\cos\theta}{(h_\theta)^3}\right\rangle + \left\langle\frac{\sin^2\theta}{(h_\theta)^2}\right\rangle + \langle P\sin\theta\cos\theta\rangle\right) - \widehat{V}_{\phi j}3\left\langle\left(\frac{1}{R}\frac{\partial R}{\partial\theta}\right)^2\frac{\sin^2\theta}{(h_\theta)^2}\right\rangle\right]$$
$$-\varepsilon\sum_{j\neq k}\overline{\nu}_{jk}^* f_p\sqrt{\frac{m_j}{m_k}}\widehat{V}_{\theta k}\langle\sin^2\theta\rangle + \widehat{V}_{rj}\varepsilon\left\langle\frac{\sin^2\theta}{(1+\varepsilon\cos\xi)}\right\rangle,$$

$$A_{S3} = \varepsilon\sum_{j\neq k}\overline{\nu}_{jk}^* f_p\widehat{V}_{\theta j}\langle\sin^2\theta\rangle,$$

$$B_S = qrf_p^2\widehat{V}_{\theta j}^2\frac{1}{\varepsilon}\left\langle\frac{1}{R}\frac{\partial R}{\partial\theta}\sin\theta\frac{1}{h_\theta}\right\rangle + qrf_p\widehat{V}_{\theta j}\widehat{V}_{\phi j}\frac{1}{\varepsilon}\left\langle\frac{1}{R}\frac{\partial R}{\partial\theta}\sin\theta\frac{1}{h_\theta}\right\rangle - \widehat{V}_{\phi j}\widetilde{V}_{\phi j}^s q^2R_0rf_jf_p\left[-\left\langle\frac{\partial h_\theta}{\partial\theta}\frac{\sin\theta\cos\theta}{(h_\theta)^3}\right\rangle - \left\langle\frac{\sin^2\theta}{(h_\theta)^2}\right\rangle\right.$$
$$\left.-3\left\langle\left(\frac{1}{R}\frac{\partial R}{\partial\theta}\right)^2\frac{\sin^2\theta}{(h_\theta)^2}\right\rangle\right] + \langle\sin\theta M_{\theta j}\rangle\frac{qR_0}{\overline{n}_j m_j V_{thj}^2} + \frac{1}{2}qr\overline{\overline{\Phi}}_j\widetilde{\Phi}^c\left\langle\frac{\sin^2\theta}{h_\theta}\right\rangle \tag{A.3}$$

where

$$\begin{aligned}\widetilde{V}_{\phi j}^c &= \alpha_j^{1C} + \frac{\widehat{\Phi}_j'}{\widehat{V}_{\phi j}}\alpha_j^{2C} + \frac{\widehat{V}_{\theta j}}{\widehat{V}_{\phi j}}\alpha_j^{3C} + \frac{\widehat{P}_j'}{\widehat{V}_{\phi j}}\alpha_j^{4C}\\ &\equiv \frac{\widehat{V}_{\theta j}}{\widehat{V}_{\phi j}}\alpha_j^{3C} + H_j^{1C} = \widetilde{n}_j^c\alpha_j^{5C} + H_j^{2C}\\ &= \frac{\widehat{V}_{\theta j}}{\widehat{V}_{\phi j}}\left[\alpha_j^{3C} + \alpha_j^{2C}\frac{\left\langle\frac{1}{1+\varepsilon\cos\xi}\right\rangle}{\left\langle\frac{1}{h_r}\right\rangle}\right] + \alpha_j^{1C} - \alpha_j^{2C}\left(1+\frac{\partial R_0(r)}{\partial r}\right)\frac{\left\langle\frac{1}{(1+\varepsilon\cos\xi)}\frac{1}{h_r}\right\rangle}{\left\langle\frac{1}{h_r}\right\rangle} - \frac{\widehat{P}_j'}{\widehat{V}_{\phi j}}\left(\alpha_j^{2C} - \alpha_j^{4C}\right)\end{aligned} \tag{A.4}$$

$$\begin{aligned}\widetilde{V}_{\phi j}^s &= \widetilde{n}_j^s\alpha_j^{1S} + \alpha_j^{2S} = -\frac{\widehat{V}_{\theta j}}{\widehat{V}_{\phi j}}\frac{\left\langle\frac{1}{1+\varepsilon\cos\xi}\right\rangle}{\left\langle\frac{1}{h_r}\right\rangle}\frac{\left\langle\sin^2\theta\frac{1}{h_r}\right\rangle}{\left(1+\frac{\partial R_0(r)}{\partial r}\right)\left\langle\frac{\sin^2\theta}{(1+\varepsilon\cos\xi)}\frac{1}{h_r}\right\rangle}\left(\widetilde{n}_j^s + \widetilde{\Phi}^s\right)\\ &+\frac{1}{\widehat{V}_{\phi j}}\left[\widehat{V}_{\phi j}\left(1+\frac{\partial R_0(r)}{\partial r}\right)\frac{\left\langle\frac{1}{(1+\varepsilon\cos\xi)}\frac{1}{h_r}\right\rangle}{\left\langle\frac{1}{h_r}\right\rangle} + \widehat{P}_j'\right]\frac{\left\langle\sin^2\theta\frac{1}{h_r}\right\rangle}{\left(1+\frac{\partial R_0(r)}{\partial r}\right)\left\langle\frac{\sin^2\theta}{(1+\varepsilon\cos\xi)}\frac{1}{h_r}\right\rangle}\left(\widetilde{n}_j^s + \widetilde{\Phi}^s\right)\\ &-\frac{1}{\widehat{V}_{\phi j}}\widetilde{n}_j^s\frac{\left\langle\sin^2\theta\frac{1}{h_r}\right\rangle}{\left(1+\frac{\partial R_0(r)}{\partial r}\right)\left\langle\frac{\sin^2\theta}{(1+\varepsilon\cos\xi)}\frac{1}{h_r}\right\rangle}\left(\widehat{P}_j' + \widehat{V}_{\phi j}\right)\end{aligned} \tag{A.5}$$

with

$$\alpha_j^{1C} \equiv -\frac{1}{\varepsilon}\frac{\left\langle\frac{\cos\theta}{(1+\varepsilon\cos\xi)}\frac{1}{h_r}\right\rangle + \varepsilon\widetilde{n}_j^c\left\langle\frac{\cos^2\theta}{(1+\varepsilon\cos\xi)}\frac{1}{h_r}\right\rangle}{\left\langle\frac{\cos^2\theta}{(1+\varepsilon\cos\xi)}\frac{1}{h_r}\right\rangle}, \qquad \alpha_j^{2C} \equiv -\frac{1}{\varepsilon}\frac{\left\langle\cos\theta\frac{1}{h_r}\right\rangle + \varepsilon\left(\widetilde{n}_j^c + \widetilde{\Phi}^c\right)\left\langle\cos^2\theta\frac{1}{h_r}\right\rangle}{\left(1+\frac{\partial R_0(r)}{\partial r}\right)\left\langle\frac{\cos^2\theta}{(1+\varepsilon\cos\xi)}\frac{1}{h_r}\right\rangle},$$

$$\alpha_j^{3C} \equiv \frac{1}{\varepsilon}\frac{\left\langle\frac{\cos\theta}{1+\varepsilon\cos\xi}\right\rangle + \frac{\left\langle\frac{1}{R}\frac{\partial R}{\partial\theta}\sin\theta\frac{1}{h_\theta}\right\rangle}{\left\langle\sin^2\theta\frac{1}{h_\theta}\right\rangle}\left\langle\frac{\cos^2\theta}{1+\varepsilon\cos\xi}\right\rangle}{\left(1+\frac{\partial R_0(r)}{\partial r}\right)\left\langle\frac{\cos^2\theta}{(1+\varepsilon\cos\xi)}\frac{1}{h_r}\right\rangle}, \qquad \alpha_j^{4C} \equiv -\frac{1}{\varepsilon}\frac{\left\langle\cos\theta\frac{1}{h_r}\right\rangle + \varepsilon\widetilde{n}_j^c\left\langle\cos^2\theta\frac{1}{h_r}\right\rangle}{\left(1+\frac{\partial R_0(r)}{\partial r}\right)\left\langle\frac{\cos^2\theta}{(1+\varepsilon\cos\xi)}\frac{1}{h_r}\right\rangle}$$

$$\alpha_j^{5C} \equiv \frac{1}{\left\langle\frac{\cos^2\theta}{(1+\varepsilon\cos\xi)}\frac{1}{h_r}\right\rangle}\left(-\left\langle\frac{\cos^2\theta}{(1+\varepsilon\cos\xi)}\frac{1}{h_r}\right\rangle - \frac{\widehat{\Phi}_j'}{\widehat{V}_{\phi j}}\frac{\left\langle\cos^2\theta\frac{1}{h_r}\right\rangle}{\left(1+\frac{\partial R_0(r)}{\partial r}\right)} - \frac{\widehat{P}_j'}{\widehat{V}_{\phi j}}\frac{\left\langle\cos^2\theta\frac{1}{h_r}\right\rangle}{\left(1+\frac{\partial R_0(r)}{\partial r}\right)}\right)$$

$$
\begin{aligned}
H_j^{1C} &\equiv \alpha_j^{1C} + \frac{\widehat{\Phi}_j'}{\widehat{V}_{\phi j}}\alpha_j^{2C} + \frac{\widehat{P}_j'}{\widehat{V}_{\phi j}}\alpha_j^{4C} \\
&= \frac{\widehat{V}_{\theta j}}{\widehat{V}_{\phi j}}\frac{\left\langle \frac{1}{1+\varepsilon\cos\xi}\right\rangle}{\left\langle \frac{1}{h_r}\right\rangle}\alpha_j^{2C} + \alpha_j^{1C} - \left(1+\frac{\partial R_0(r)}{\partial r}\right)\frac{\left\langle \frac{1}{(1+\varepsilon\cos\xi)}\frac{1}{h_r}\right\rangle}{\left\langle \frac{1}{h_r}\right\rangle}\alpha_j^{2C} - \frac{\widehat{P}_j'}{\widehat{V}_{\phi j}}\left(\alpha_j^{2C}-\alpha_j^{4C}\right) \\
H_j^{2C} &\equiv -\frac{1}{\varepsilon\left\langle \frac{\cos^2\theta}{(1+\varepsilon\cos\xi)}\frac{1}{h_r}\right\rangle}\left[\left\langle \frac{\cos\theta}{(1+\varepsilon\cos\xi)}\frac{1}{h_r}\right\rangle \right. \\
&\quad \left. + \frac{\widehat{\Phi}_j'}{\widehat{V}_{\phi j}}\frac{1}{\left(1+\frac{\partial R_0(r)}{\partial r}\right)}\left(\left\langle \cos\theta\frac{1}{h_r}\right\rangle + \varepsilon\widetilde{\Phi}^c\left\langle \cos^2\theta\frac{1}{h_r}\right\rangle\right) + \frac{\widehat{P}_j'}{\widehat{V}_{\phi j}}\frac{\left\langle \cos\theta\frac{1}{h_r}\right\rangle}{\left(1+\frac{\partial R_0(r)}{\partial r}\right)}\right] + \frac{\widehat{V}_\theta}{\widehat{V}_\phi}\alpha_j^{3c} \\
\alpha_j^{1S} &\equiv -\frac{\left\langle \sin^2\theta\frac{1}{h_r}\right\rangle}{\left(1+\frac{\partial R_0(r)}{\partial r}\right)\left\langle \frac{\sin^2\theta}{(1+\varepsilon\cos\xi)}\frac{1}{h_r}\right\rangle}\left(\frac{\widehat{\Phi}_j'}{\widehat{V}_{\phi j}} + \frac{\widehat{P}_j'}{\widehat{V}_{\phi j}} + 1\right), \qquad \alpha_j^{2S} \equiv -\frac{\widehat{\Phi}_j'}{\widehat{V}_{\phi j}}\widetilde{\Phi}^s\frac{\left\langle \sin^2\theta\frac{1}{h_r}\right\rangle}{\left(1+\frac{\partial R_0(r)}{\partial r}\right)\left\langle \frac{\sin^2\theta}{(1+\varepsilon\cos\xi)}\frac{1}{h_r}\right\rangle}.
\end{aligned}
$$

Here $\partial R_0(r)/\partial r$ is the Shafranov shift, given in Ref. [1]. Note that Eqs. (A.4) and (A.5) are expressed in several forms to make it easy to couple them with different moments in Eqs. (A.1)–(A.3).

Appendix B. Coefficients in the numerical calculation model

The coefficients of the final numerical code come from the coefficients in Appendix A updated with the coupling relations between $\widetilde{V}_{\phi j}^{c,s}$ and $\widetilde{n}_j^{c,s}$, Eqs. (A.4) and (A.5).

B.1. Coefficients in the density asymmetry subsystem

$$
\begin{aligned}
a_{11} &= q^2R_0rf_if_p\left[\left(\frac{1}{3}\widehat{V}_{\theta i}+\widehat{V}_{\phi i}\alpha_i^{5C}\right)\left[\left\langle\frac{\partial h_\theta}{\partial\theta}\frac{\sin\theta\cos\theta}{(h_\theta)^3}\right\rangle - \left\langle\frac{\cos^2\theta}{(h_\theta)^2}\right\rangle\right]\right] - \left(\overline{\nu}_{il}^* + \overline{\nu}_{ie}^*\right)\varepsilon f_p\sqrt{\frac{m_i}{m_I}}\widehat{V}_{\theta I}\left\langle\cos^2\theta\right\rangle + \widehat{V}_{ri}\varepsilon\left\langle\frac{\cos^2\theta}{(1+\varepsilon\cos\xi)}\right\rangle \\
a_{12} &= qr\left[-f_p\widehat{V}_{\theta i}\left(f_p\widehat{V}_{\theta i}\left\langle\frac{\cos^2\theta}{h_\theta}\right\rangle + \widehat{V}_{\phi i}\alpha_i^{1S}\left\langle\frac{1}{R}\frac{\partial R}{\partial\theta}\frac{\sin\theta\cos\theta}{h_\theta}\right\rangle\right) + \frac{1}{2}\left\langle\frac{\cos^2\theta}{h_\theta}\right\rangle\right] \\
a_{13} &= \left(\overline{\nu}_{il}^* + \overline{\nu}_{ie}^*\right)\varepsilon f_p\widehat{V}_{\theta i}\left\langle\cos^2\theta\right\rangle, \qquad a_{14} = 0 \\
b_1 &= qrf_p\widehat{V}_{\theta i}\widehat{V}_{\phi i}\alpha_i^{2S}\left\langle\frac{1}{R}\frac{\partial R}{\partial\theta}\frac{\sin\theta\cos\theta}{h_\theta}\right\rangle - q^2{R_0}^2f_if_p\widehat{V}_{\theta i}\left[\frac{\left\langle\frac{1}{R}\frac{\partial R}{\partial\theta}\frac{\sin\theta}{h_\theta}\right\rangle}{\left\langle\frac{\sin^2\theta}{h_\theta}\right\rangle}\left(-\frac{1}{3}\left\langle\frac{\partial h_\theta}{\partial\theta}\frac{\sin\theta\cos\theta}{(h_\theta)^3}\right\rangle\right.\right. \\
&\quad \left.\left. + \frac{1}{3}\left\langle\frac{\cos^2\theta}{(h_\theta)^2}\right\rangle + \left\langle M\cos^2\theta\right\rangle - \left\langle P\sin\theta\cos\theta\right\rangle\right) + \left\langle M\cos\theta\right\rangle + 3\left\langle Q\cos\theta\right\rangle\right] - q^2{R_0}^2f_if_p\widehat{V}_{\phi i}\left[\varepsilon H_i^{2C}\left(\left\langle\frac{\partial h_\theta}{\partial\theta}\frac{\sin\theta\cos\theta}{(h_\theta)^3}\right\rangle\right.\right. \\
&\quad \left.\left. - \left\langle\frac{\cos^2\theta}{(h_\theta)^2}\right\rangle - \left\langle N\cos^2\theta\right\rangle\right) - \left\langle N\cos\theta\right\rangle\right] - \left(\overline{\nu}_{il}^* + \overline{\nu}_{ie}^*\right)f_p\left(\widehat{V}_{\theta i} - \sqrt{\frac{m_i}{m_I}}\widehat{V}_{\theta I}\right)\left[\left\langle\cos\theta\right\rangle + \frac{\left\langle\frac{1}{R}\frac{\partial R}{\partial\theta}\frac{\sin\theta}{h_\theta}\right\rangle}{\left\langle\frac{\sin^2\theta}{h_\theta}\right\rangle}\left\langle\cos^2\theta\right\rangle\right] \\
&\quad - \widehat{V}_{ri}\left\langle\frac{\cos\theta}{(1+\varepsilon\cos\xi)}\right\rangle - \frac{1}{2}qr\overline{\overline{\Phi}}_i\widetilde{\Phi}^s\left\langle\frac{\cos^2\theta}{h_\theta}\right\rangle - f_p\nu_{\text{atomi}}^*\widehat{V}_{\theta i}\left(\left\langle\cos\theta\right\rangle + \frac{\left\langle\frac{1}{R}\frac{\partial R}{\partial\theta}\frac{\sin\theta}{h_\theta}\right\rangle}{\left\langle\frac{\sin^2\theta}{h_\theta}\right\rangle}\left\langle\cos^2\theta\right\rangle\right) + \left\langle\cos\theta M_{\theta i}\right\rangle\frac{qR_0}{\overline{n}_im_iV_{thi}^2} \qquad \text{(B.1)} \\
a_{21} &= qr\left(f_p^2\widehat{V}_{\theta i}^2 - \frac{1}{2}\right)\left\langle\frac{\sin^2\theta}{h_\theta}\right\rangle \\
a_{22} &= q^2R_0rf_if_p\left\{-\left(\frac{1}{3}\widehat{V}_{\theta i}+\widehat{V}_{\phi i}\alpha_i^{1S}\right)\left[\left\langle\frac{\partial h_\theta}{\partial\theta}\frac{\sin\theta\cos\theta}{(h_\theta)^3}\right\rangle + \left\langle\frac{\sin^2\theta}{(h_\theta)^2}\right\rangle\right]\right. \\
&\quad \left. - \frac{1}{3}\widehat{V}_{\theta i}\left\langle P\sin\theta\cos\theta\right\rangle - 3\left(\widehat{V}_{\phi i}\alpha_i^{1S} + \widehat{V}_{\phi i}\right)\left\langle\left(\frac{1}{R}\frac{\partial R}{\partial\theta}\right)^2\frac{\sin^2\theta}{(h_\theta)^2}\right\rangle\right\} + \widehat{V}_{ri}\varepsilon\left\langle\frac{\sin^2\theta}{(1+\varepsilon\cos\xi)}\right\rangle - \varepsilon\left(\overline{\nu}_{il}^* + \overline{\nu}_{ie}^*\right)f_p\sqrt{\frac{m_i}{m_I}}\widehat{V}_{\theta I}\left\langle\sin^2\theta\right\rangle \\
a_{23} &= 0, \qquad a_{24} = \varepsilon\left(\overline{\nu}_{il}^* + \overline{\nu}_{ie}^*\right)f_p\widehat{V}_{\theta i}\left\langle\sin^2\theta\right\rangle \approx \varepsilon\left(\overline{\nu}_{il}^* + \overline{\nu}_{ie}^*\right)f_p\widehat{V}_{\theta i}\left\langle\cos^2\theta\right\rangle \\
b_2 &= qR_0f_p\widehat{V}_{\theta i}\left(f_p\widehat{V}_{\theta i} + \widehat{V}_{\phi i}\right)\left\langle\frac{1}{R}\frac{\partial R}{\partial\theta}\frac{\sin\theta}{h_\theta}\right\rangle + q^2R_0rf_if_p\widehat{V}_{\phi i}\alpha_i^{2S}\left(\left\langle\frac{\partial h_\theta}{\partial\theta}\frac{\sin\theta\cos\theta}{(h_\theta)^3}\right\rangle\right. \\
&\quad \left. + \left\langle\frac{\sin^2\theta}{(h_\theta)^2}\right\rangle + 3\left\langle\left(\frac{1}{R}\frac{\partial R}{\partial\theta}\right)^2\frac{\sin^2\theta}{(h_\theta)^2}\right\rangle\right) + \frac{1}{2}qr\overline{\overline{\Phi}}_i\widetilde{\Phi}^c\left\langle\frac{\sin^2\theta}{h_\theta}\right\rangle + \left\langle\sin\theta M_{\theta i}\right\rangle\frac{qR_0}{\overline{n}_im_iV_{thi}^2} \qquad \text{(B.2)}
\end{aligned}
$$

$$a_{31} = \left(\overline{\nu}_{Ii}^{*} + \overline{\nu}_{Ie}^{*}\right) \varepsilon f_p \widehat{V}_{\theta I} \left\langle \cos^2\theta \right\rangle, \qquad a_{32} = 0$$

$$a_{33} = q^2 R_0 r f_I f_p \left[\left(\frac{1}{3}\widehat{V}_{\theta I} + \widehat{V}_{\phi I}\alpha_I^{5C} \right) \left[\left\langle \frac{\partial h_\theta}{\partial\theta} \frac{\sin\theta\cos\theta}{(h_\theta)^3} \right\rangle - \left\langle \frac{\cos^2\theta}{(h_\theta)^2} \right\rangle \right] \right]$$
$$- \left(\overline{\nu}_{Ii}^{*} + \overline{\nu}_{Ie}^{*}\right) \varepsilon f_p \sqrt{\frac{m_I}{m_i}} \widehat{V}_{\theta i} \left\langle \cos^2\theta \right\rangle + \widehat{V}_{rI}\varepsilon \left\langle \frac{\cos^2\theta}{(1+\varepsilon\cos\xi)} \right\rangle$$

$$a_{34} = qr \left[-f_p \widehat{V}_{\theta I} \left(f_p \widehat{V}_{\theta I} \left\langle \frac{\cos^2\theta}{h_\theta} \right\rangle + \widehat{V}_{\phi I}\alpha_I^{1S} \left\langle \frac{1}{R}\frac{\partial R}{\partial\theta} \frac{\sin\theta\cos\theta}{h_\theta} \right\rangle \right) + \frac{1}{2} \left\langle \frac{\cos^2\theta}{h_\theta} \right\rangle \right]$$

$$b_3 = qr f_p \widehat{V}_{\theta I} \widehat{V}_{\phi I} \alpha_I^{2S} \left\langle \frac{1}{R}\frac{\partial R}{\partial\theta} \frac{\sin\theta\cos\theta}{h_\theta} \right\rangle - q^2 {R_0}^2 f_I f_p \widehat{V}_{\theta I} \left[\frac{\left\langle \frac{1}{R}\frac{\partial R}{\partial\theta}\frac{\sin\theta}{h_\theta} \right\rangle}{\left\langle \frac{\sin^2\theta}{h_\theta} \right\rangle} \left(-\frac{1}{3} \left\langle \frac{\partial h_\theta}{\partial\theta} \frac{\sin\theta\cos\theta}{(h_\theta)^3} \right\rangle + \frac{1}{3} \left\langle \frac{\cos^2\theta}{(h_\theta)^2} \right\rangle \right.\right.$$
$$\left.\left. + \left\langle M\cos^2\theta \right\rangle - \left\langle P\sin\theta\cos\theta \right\rangle \right) + \left\langle M\cos\theta \right\rangle + 3\left\langle Q\cos\theta \right\rangle \right] - q^2 {R_0}^2 f_I f_p \widehat{V}_{\phi I} \left[\varepsilon H_I^{2C} \left(\left\langle \frac{\partial h_\theta}{\partial\theta} \frac{\sin\theta\cos\theta}{(h_\theta)^3} \right\rangle \right.\right.$$
$$\left.\left. - \left\langle \frac{\cos^2\theta}{(h_\theta)^2} \right\rangle - \left\langle N\cos^2\theta \right\rangle \right) - \left\langle N\cos\theta \right\rangle \right] - \left(\overline{\nu}_{Ii}^{*} + \overline{\nu}_{Ie}^{*}\right) f_p \left(\widehat{V}_{\theta I} - \sqrt{\frac{m_I}{m_i}} \widehat{V}_{\theta i} \right) \left[\left\langle \cos\theta \right\rangle + \frac{\left\langle \frac{1}{R}\frac{\partial R}{\partial\theta}\frac{\sin\theta}{h_\theta} \right\rangle}{\left\langle \frac{\sin^2\theta}{h_\theta} \right\rangle} \left\langle \cos^2\theta \right\rangle \right]$$
$$- \widehat{V}_{rI} \left\langle \frac{\cos\theta}{(1+\varepsilon\cos\xi)} \right\rangle - \frac{1}{2} qr \overline{\overline{\Phi}}_I \widetilde{\Phi}^s \left\langle \frac{\cos^2\theta}{h_\theta} \right\rangle - f_p \nu_{\text{atom}I}^{*} \widehat{V}_{\theta I} \left(\left\langle \cos\theta \right\rangle + \frac{\left\langle \frac{1}{R}\frac{\partial R}{\partial\theta}\frac{\sin\theta}{h_\theta} \right\rangle}{\left\langle \frac{\sin^2\theta}{h_\theta} \right\rangle} \left\langle \cos^2\theta \right\rangle \right) + \left\langle \cos\theta M_{\theta I} \right\rangle \frac{qR_0}{\overline{n}_I m_I V_{thI}^2} \tag{B.3}$$

$$a_{41} = 0, \qquad a_{42} = \varepsilon \left(\overline{\nu}_{Ii}^{*} + \overline{\nu}_{Ie}^{*}\right) f_p \widehat{V}_{\theta I} \left\langle \sin^2\theta \right\rangle \approx \varepsilon \left(\overline{\nu}_{Ii}^{*} + \overline{\nu}_{Ie}^{*}\right) f_p \widehat{V}_{\theta I} \left\langle \cos^2\theta \right\rangle$$

$$a_{43} = qr \left(f_p^2 \widehat{V}_{\theta I}^2 - \frac{1}{2} \right) \left\langle \frac{\sin^2\theta}{h_\theta} \right\rangle$$

$$a_{44} = q^2 R_0 r f_I f_p \left\{ - \left(\frac{1}{3}\widehat{V}_{\theta I} + \widehat{V}_{\phi I}\alpha_I^{1S} \right) \left[\left\langle \frac{\partial h_\theta}{\partial\theta} \frac{\sin\theta\cos\theta}{(h_\theta)^3} \right\rangle + \left\langle \frac{\sin^2\theta}{(h_\theta)^2} \right\rangle \right] \right.$$
$$\left. - \frac{1}{3}\widehat{V}_{\theta I} \left\langle P\sin\theta\cos\theta \right\rangle - 3\left(\widehat{V}_{\phi I}\alpha_I^{1S} + \widehat{V}_{\phi I} \right) \left\langle \left(\frac{1}{R}\frac{\partial R}{\partial\theta} \right)^2 \frac{\sin^2\theta}{(h_\theta)^2} \right\rangle \right\} + \widehat{V}_{rI}\varepsilon \left\langle \frac{\sin^2\theta}{(1+\varepsilon\cos\xi)} \right\rangle - \varepsilon \left(\overline{\nu}_{Ii}^{*} + \overline{\nu}_{Ie}^{*}\right) f_p \sqrt{\frac{m_I}{m_i}} \widehat{V}_{\theta i} \left\langle \sin^2\theta \right\rangle$$

$$b_4 = qR_0 f_p \widehat{V}_{\theta I} \left(f_p \widehat{V}_{\theta I} + \widehat{V}_{\phi I} \right) \left\langle \frac{1}{R}\frac{\partial R}{\partial\theta}\frac{\sin\theta}{h_\theta} \right\rangle + q^2 R_0 r f_I f_p \widehat{V}_{\phi I} \alpha_I^{2S} \left(\left\langle \frac{\partial h_\theta}{\partial\theta} \frac{\sin\theta\cos\theta}{(h_\theta)^3} \right\rangle \right.$$
$$\left. + \left\langle \frac{\sin^2\theta}{(h_\theta)^2} \right\rangle + 3\left\langle \left(\frac{1}{R}\frac{\partial R}{\partial\theta} \right)^2 \frac{\sin^2\theta}{(h_\theta)^2} \right\rangle \right) + \frac{1}{2} qr \overline{\overline{\Phi}}_I \widetilde{\Phi}^c \left\langle \frac{\sin^2\theta}{h_\theta} \right\rangle + \left\langle \sin\theta M_{\theta I} \right\rangle \frac{qR_0}{\overline{n}_I m_I V_{thI}^2} \tag{B.4}$$

B.2. Coefficients in the poloidal rotation subsystem

$$c_{11} = \widehat{V}_{\theta i}^{n-1} qr f_p^2 \widetilde{n}_i^s \left(\left\langle \frac{\cos\theta}{h_\theta} \right\rangle + \frac{\left\langle \frac{1}{R}\frac{\partial R}{\partial\theta}\frac{\sin\theta}{h_\theta} \right\rangle}{\left\langle \frac{\sin^2\theta}{h_\theta} \right\rangle} \left\langle \frac{\cos^2\theta}{h_\theta} \right\rangle \right) + qr f_p \widehat{V}_{\phi i} \widetilde{V}_{\phi i}^s \left\langle \frac{1}{R}\frac{\partial R}{\partial\theta}\frac{\sin\theta}{h_\theta} \right\rangle - f_p \left(\overline{\nu}_{iI}^{*} + \overline{\nu}_{ie}^{*}\right)$$
$$- f_p \nu_{\text{atom}i}^{*} - q^2 {R_0}^2 f_i f_p \left[\left(\frac{1}{3}\widetilde{n}_i^c + \alpha_i^{3C} \right) \varepsilon \left\langle \frac{\partial h_\theta}{\partial\theta} \frac{\sin\theta}{(h_\theta)^3} \right\rangle - \left(\widetilde{n}_i^c + 2\alpha_i^{3C} \right) \varepsilon \left\langle \frac{1}{R}\frac{\partial R}{\partial\theta} \frac{\sin\theta}{(h_\theta)^2} \right\rangle \right.$$
$$- \left(\widetilde{n}_i^c + \alpha_i^{3C} \right) \frac{1}{3}\varepsilon \left\langle \frac{\cos\theta}{(h_\theta)^2} \right\rangle + 3\left\langle Q \right\rangle + \left\langle M \right\rangle - \alpha_i^{3C}\varepsilon \left\langle N\cos\theta \right\rangle + \frac{\left\langle \frac{1}{R}\frac{\partial R}{\partial\theta}\sin\theta\frac{1}{h_\theta} \right\rangle}{\left\langle \frac{\sin^2\theta}{h_\theta} \right\rangle} \left(-\frac{1}{3} \left\langle \frac{\partial h_\theta}{\partial\theta} \frac{\sin\theta}{(h_\theta)^3} \right\rangle + \left\langle \frac{1}{R}\frac{\partial R}{\partial\theta} \frac{\sin\theta}{(h_\theta)^2} \right\rangle \right.$$
$$\left.\left. + \frac{1}{3} \left\langle \frac{\cos\theta}{(h_\theta)^2} \right\rangle + \left\langle M\cos\theta \right\rangle - \left\langle P\sin\theta \right\rangle \right) \right] + q^2 {R_0}^2 f_i f_p \varepsilon \frac{\left\langle \frac{1}{1+\varepsilon\cos\xi} \right\rangle}{\left\langle \frac{1}{h_r} \right\rangle} \alpha_i^{2C} \left(2\left\langle \frac{1}{R}\frac{\partial R}{\partial\theta}\frac{\sin\theta}{(h_\theta)^2} \right\rangle \right.$$
$$\left. + \left\langle N\cos\theta \right\rangle - \left\langle \frac{\partial h_\theta}{\partial\theta} \frac{\sin\theta}{(h_\theta)^3} \right\rangle + \left\langle \frac{\cos\theta}{(h_\theta)^2} \right\rangle \right)$$

$$c_{12} = f_p \left(\overline{\nu}_{iI}^{*} + \overline{\nu}_{ie}^{*}\right) \sqrt{\frac{m_i}{m_I}}$$

$$d_1 = q^2 {R_0}^2 \widehat{V}_{\phi i} f_i f_p \left[\widetilde{n}_i^c \varepsilon \left(\left\langle \frac{1}{R}\frac{\partial R}{\partial\theta} \frac{\sin\theta}{(h_\theta)^2} \right\rangle - \left\langle N\cos\theta \right\rangle \right) - \left\langle N \right\rangle - 3\left\langle \left(\frac{1}{R}\frac{\partial R}{\partial\theta} \right)^2 \frac{1}{(h_\theta)^2} \right\rangle \right.$$

$$+\varepsilon\left(\alpha_i^{1C}-\left(1+\frac{\partial R_0(r)}{\partial r}\right)\frac{\left\langle\frac{1}{(1+\varepsilon\cos\xi)}\frac{1}{h_r}\right\rangle}{\left\langle\frac{1}{h_r}\right\rangle}\alpha_i^{2C}-\frac{\widehat{P}_i}{\widehat{V}_{\phi i}}\left(\alpha_i^{2C}-\alpha_i^{4C}\right)\right)\left(-2\left\langle\frac{1}{R}\frac{\partial R}{\partial\theta}\frac{\sin\theta}{(h_\theta)^2}\right\rangle\right.$$
$$\left.-\langle N\cos\theta\rangle+\left\langle\frac{\partial h_\theta}{\partial\theta}\frac{\sin\theta}{(h_\theta)^3}\right\rangle-\left\langle\frac{\cos\theta}{(h_\theta)^2}\right\rangle\right)\Bigg]+\frac{1}{2}qr\widetilde{n}_i^s\left\langle\frac{\cos\theta}{h_\theta}\right\rangle-\langle M_{\theta i}\rangle\frac{qR_0}{\overline{n}_i m_i V_{thi}^2}$$
$$+\widehat{V}_{ri}\left\langle\frac{1}{(1+\varepsilon\cos\xi)}\right\rangle+\frac{1}{2}qR_0\overline{\overline{\Phi}}_i\varepsilon\left[\widetilde{\Phi}^s\left(\left\langle\frac{\cos\theta}{h_\theta}\right\rangle+\varepsilon\widetilde{n}_i^c\left\langle\frac{\cos^2\theta}{h_\theta}\right\rangle\right)-\varepsilon\widetilde{n}_i^s\widetilde{\Phi}^c\left\langle\frac{\sin^2\theta}{h_\theta}\right\rangle\right] \tag{B.5}$$

$$c_{21}=f_p\left(\overline{v}_{Ii}^*+\overline{v}_{Ie}^*\right)\sqrt{\frac{m_I}{m_i}}$$

$$c_{22}=\widehat{V}_{\theta I}^{n-1}qrf_p^2\widetilde{n}_I^s\left(\left\langle\frac{\cos\theta}{h_\theta}\right\rangle+\frac{\left\langle\frac{1}{R}\frac{\partial R}{\partial\theta}\frac{\sin\theta}{h_\theta}\right\rangle}{\left\langle\frac{\sin^2\theta}{h_\theta}\right\rangle}\left\langle\frac{\cos^2\theta}{h_\theta}\right\rangle\right)+qrf_p\widehat{V}_{\phi I}\widetilde{V}_{\phi I}^s\left\langle\frac{1}{R}\frac{\partial R}{\partial\theta}\frac{\sin\theta}{h_\theta}\right\rangle-f_p\left(\overline{v}_{Ii}^*+\overline{v}_{Ie}^*\right)$$
$$-f_p\nu_{\mathrm{atom}I}^*-q^2{R_0}^2f_If_p\left[\left(\frac{1}{3}\widetilde{n}_I^c+\alpha_I^{3C}\right)\varepsilon\left\langle\frac{\partial h_\theta}{\partial\theta}\frac{\sin\theta}{(h_\theta)^3}\right\rangle-\left(\widetilde{n}_I^c+2\alpha_I^{3C}\right)\varepsilon\left\langle\frac{1}{R}\frac{\partial R}{\partial\theta}\frac{\sin\theta}{(h_\theta)^2}\right\rangle\right.$$
$$-\left(\widetilde{n}_I^c+\alpha_I^{3C}\right)\frac{1}{3}\varepsilon\left\langle\frac{\cos\theta}{(h_\theta)^2}\right\rangle+3\langle Q\rangle+\langle M\rangle-\alpha_I^{3C}\varepsilon\langle N\cos\theta\rangle+\frac{\left\langle\frac{1}{R}\frac{\partial R}{\partial\theta}\sin\theta\frac{1}{h_\theta}\right\rangle}{\left\langle\frac{\sin^2\theta}{h_\theta}\right\rangle}$$
$$\left.\times\left(-\frac{1}{3}\left\langle\frac{\partial h_\theta}{\partial\theta}\frac{\sin\theta}{(h_\theta)^3}\right\rangle+\left\langle\frac{1}{R}\frac{\partial R}{\partial\theta}\frac{\sin\theta}{(h_\theta)^2}\right\rangle+\frac{1}{3}\left\langle\frac{\cos\theta}{(h_\theta)^2}\right\rangle+\langle M\cos\theta\rangle-\langle P\sin\theta\rangle\right)\right]$$
$$+q^2{R_0}^2f_If_p\varepsilon\frac{\left\langle\frac{1}{1+\varepsilon\cos\xi}\right\rangle}{\left\langle\frac{1}{h_r}\right\rangle}\alpha_I^{2C}\left(2\left\langle\frac{1}{R}\frac{\partial R}{\partial\theta}\frac{\sin\theta}{(h_\theta)^2}\right\rangle+\langle N\cos\theta\rangle-\left\langle\frac{\partial h_\theta}{\partial\theta}\frac{\sin\theta}{(h_\theta)^3}\right\rangle+\left\langle\frac{\cos\theta}{(h_\theta)^2}\right\rangle\right)$$

$$d_2=q^2{R_0}^2\widehat{V}_{\phi I}f_If_p\left[\widetilde{n}_I^c\varepsilon\left(\left\langle\frac{1}{R}\frac{\partial R}{\partial\theta}\frac{\sin\theta}{(h_\theta)^2}\right\rangle-\langle N\cos\theta\rangle\right)-\langle N\rangle-3\left\langle\left(\frac{1}{R}\frac{\partial R}{\partial\theta}\right)^2\frac{1}{(h_\theta)^2}\right\rangle\right.$$
$$+\varepsilon\left(\alpha_I^{1C}-\left(1+\frac{\partial R_0(r)}{\partial r}\right)\frac{\left\langle\frac{1}{(1+\varepsilon\cos\xi)}\frac{1}{h_r}\right\rangle}{\left\langle\frac{1}{h_r}\right\rangle}\alpha_I^{2C}-\frac{\widehat{P}_I}{\widehat{V}_{\phi I}}\left(\alpha_I^{2C}-\alpha_I^{4C}\right)\right)\left(-2\left\langle\frac{1}{R}\frac{\partial R}{\partial\theta}\frac{\sin\theta}{(h_\theta)^2}\right\rangle\right.$$
$$\left.\left.-\langle N\cos\theta\rangle+\left\langle\frac{\partial h_\theta}{\partial\theta}\frac{\sin\theta}{(h_\theta)^3}\right\rangle-\left\langle\frac{\cos\theta}{(h_\theta)^2}\right\rangle\right)\right]+\frac{1}{2}qr\widetilde{n}_I^s\left\langle\frac{\cos\theta}{h_\theta}\right\rangle-\langle M_{\theta I}\rangle\frac{qR_0}{\overline{n}_I m_I V_{thI}^2}$$
$$+\widehat{V}_{rI}\left\langle\frac{1}{(1+\varepsilon\cos\xi)}\right\rangle+\frac{1}{2}qR_0\overline{\overline{\Phi}}_I\varepsilon\left[\widetilde{\Phi}^s\left(\left\langle\frac{\cos\theta}{h_\theta}\right\rangle+\varepsilon\widetilde{n}_I^c\left\langle\frac{\cos^2\theta}{h_\theta}\right\rangle\right)-\varepsilon\widetilde{n}_I^s\widetilde{\Phi}^c\left\langle\frac{\sin^2\theta}{h_\theta}\right\rangle\right]. \tag{B.6}$$

B.3. Coefficients in the toroidal rotation subsystem

$$e_{11}=\sqrt{\frac{m_I}{m_i}}\beta_i,\qquad e_{12}=\beta_I,\qquad f_1=\frac{y_i+y_I}{V_{thI}} \tag{B.7}$$

$$e_{21}=1,\qquad e_{22}=-\sqrt{\frac{m_i}{m_I}}$$
$$f_2=\left(\widehat{V}_{\theta i}-\sqrt{\frac{m_i}{m_I}}\widehat{V}_{\theta I}\right)\frac{\left\langle\frac{1}{1+\varepsilon\cos\xi}\right\rangle}{\left(1+\frac{\partial R_0(r)}{\partial r}\right)\left\langle\frac{1}{(1+\varepsilon\cos\xi)}\frac{1}{h_r}\right\rangle}+\left(-\widehat{P}_i+\sqrt{\frac{m_i}{m_I}}\widehat{P}_I\right)\frac{\left\langle\frac{1}{h_r}\right\rangle}{\left(1+\frac{\partial R_0(r)}{\partial r}\right)\left\langle\frac{1}{(1+\varepsilon\cos\xi)}\frac{1}{h_r}\right\rangle}. \tag{B.8}$$

References

[1] C. Bae, W.M. Stacey, W.M. Solomon, Nuclear Fusion 53 (2013) 043011.
[2] W.M. Stacey, Fusion Plasma Physics, Wiley-VCH, John Wiley, Weinheim, Chichester, 2005.
[3] R.L. Miller, M.S. Chu, J.M. Greene, Y.R. Lin-Liu, R.E. Waltz, Physics of Plasmas 5 (1998) 973–978.
[4] C.T. Kelley, Iterative Methods for Linear and Nonlinear Equations, in: Frontiers in Applied Mathematics, vol. 16, Society for Industrial and Applied Mathematics, Philadelphia, PA, 1995. SIAM 3600 Market Street, Floor 6, Philadelphia, PA 19104.
[5] J.M. Ortega, W.C. Rheinboldt, Iterative Solution of Nonlinear Equations in Several Variables, in: Classics in Applied Mathematics, vol. 30, Society for Industrial and Applied Mathematics, Philadelphia, PA, 2000. SIAM 3600 Market Street, Floor 6, Philadelphia, PA 19104.
[6] J.F. Traub, Iterative Methods for the Solution of Equations, Prentice-Hall, Englewood Cliffs, NJ, 1964.
[7] S. Kirkpatrick, C.D. Gelatt, M.P. Vecchi, Science 220 (1983) 671–680.

[8] D. Bertsimas, J.N. Tsitsiklis, Introduction to Linear Optimization, Athena Scientific, Belmont, Mass, 1997.
[9] W.M. Stacey, R.W. Johnson, J. Mandrekas, Physics of Plasmas 13 (2006) 062508.
[10] W.A. Houlberg, K.C. Shaing, S.P. Hirshman, M.C. Zarnstorff, Physics of Plasmas 4 (1997) 3230–3242.
[11] S.P. Hirshman, D.J. Sigmar, Nuclear Fusion 21 (1981) 1079–1201.
[12] Y.B. Kim, P.H. Diamond, R.J. Groebner, Physics of Fluids B (Plasma Physics) 3 (1991) 2050–2060.
[13] W.M. Stacey, D.J. Sigmar, Physics of Fluids 28 (1985) 2800–2807.
[14] W.M. Stacey, C. Bae, Physics of Plasmas 16 (2009) 082501.
[15] S.I. Braginskii, Review of Plasma Physics 1 (1965) 205.
[16] J. Candy, Plasma Physics and Controlled Fusion 51 (2009) 105009.
[17] W.M. Stacey, Physics of Plasmas 15 (2008) 122505.
[18] L. Guazzotto, R. Betti, Physical Review Letters 107 (2011) 125002.
[19] G.H. Golub, C.F. Van Loan, Matrix Computations, third ed., Johns Hopkins University Press, Baltimore, 1996.
[20] D.G. Luenberger, Linear and Nonlinear Programming, second ed., Springer, New York, NY, 2005.
[21] W.C. Rheinboldt, Methods for Solving Systems of Nonlinear Equations, second ed., Society for Industrial and Applied Mathematics, Philadelphia, 1998.
[22] J.R. Shewchuk, An Introduction to the Conjugate Gradient Method without Agonizing Pain, Carnegie Mellon University, Pittsburgh, 1994.
[23] S.H. Strogatz, Nonlinear Dynamics and Chaos: With Applications to Physics, Biology, Chemistry, and Engineering, Addison-Wesley Pub., Reading, Mass, 1994.
[24] W.M. Stacey, R.J. Groebner, Physics of Plasmas 15 (2008) 012503.
[25] J.I. Choi, Applications of nonlinear dynamics in atomic and molecular systems, 2007.
[26] B.A. Grierson, K.H. Burrell, W.M. Solomon, N.A. Pablant, Review of Scientific Instruments 81 (2010).
[27] F.L. Hinton, S.K. Wong, Physics of Fluids 28 (1985) 3082–3098.
[28] P.J. Catto, A.N. Simakov, Physics of Plasmas 11 (2004) 90–102.
[29] P.J. Catto, A.N. Simakov, Physics of Plasmas 12 (2005) 012501.
[30] A.B. Mikhailovskii, V.S. Tsypin, Soviet Journal of Plasma Physics 10 (1984) 51.
[31] J.J. Ramos, Physics of Plasmas 12 (2005) 112301.